

Proposal of a Microstrip Patch Antenna Array for the Osseus: An Equipment for the Aid of Diagnosis of Osteometabolic Diseases

Bruno Pinheiro (✉ bruno.melo@lais.huol.ufm.br)

Federal University of Rio Grande do Norte

Antônio Luiz Campos

Federal University of Rio Grande do Norte

Dionísio Dias Carvalho

Federal University of Rio Grande do Norte

Agnaldo Cruz

Federal University of Rio Grande do Norte

Ricardo Alexsandro Valentim

Federal University of Rio Grande do Norte

Nicolas Vinícius Veras

Federal University of Rio Grande do Norte

João Paulo dos Santos

Instituto Federal do Rio Grande do Norte

Research Article

Keywords: Microstrip patch antenna, osteoporosis, biotelemetry, fracture, engineering, radio frequency

Posted Date: May 4th, 2021

DOI: <https://doi.org/10.21203/rs.3.rs-453022/v1>

License: © ⓘ This work is licensed under a Creative Commons Attribution 4.0 International License.

[Read Full License](#)

Proposal of a microstrip patch antenna array for the Osseus: An equipment for the aid of diagnosis of osteometabolic diseases

Bruno de Melo Pinheiro¹ (bruno.melo@lais.huol.ufrn.br) **corresponding author**,

Antônio Luiz Pereira de Siqueira Campos¹ (alpscampos@gmail.com),

Dionísio Dias Aires de Carvalho¹ (dionisio.carvalho@navi.ifrn.edu.br),

Agnaldo Souza Cruz¹ (agnaldo.cruz@lais.huol.ufrn.br),

Ricardo Alexsandro de Medeiros Valentim¹ (ricardo.valentim@lais.huol.ufrn.br),

Nicolas Vinícius Rodrigues Veras¹ (nicolas.vinicius@lais.huol.ufrn.br),

João Paulo Queiroz dos Santos² (joao.queiroz@navi.ifrn.edu.br).

Authors' affiliation:

1:

Instituto Federal do Rio Grande do Norte BR

Campus Universitário Lagoa Nova

CEP 59078-970

Caixa postal 1524

Natal/RN – Brazil

2:

Federal Institute of Education Science and Technology

Rua Dr. Nilo Bezerra Ramalho, 1692, Tirol

CEP 59015-300

Natal/RN – Brazil

Abstract

Background

Applications on electromagnetic waves in the field of biotelemetry have increased in the latest years, being used to prevent, diagnose, and treatment of several diseases. In this context, biotelemetry allows minimally invasive monitoring of the physiologic, improving the comfort and patient care and significantly reducing hospital costs. Aiming to assist the mineral bone density classification, through a radio frequency signal (RF), for a later diagnosis of osteoporosis, Osseus was proposed in 2018. This equipment is a combination of the application of techniques and concepts of several areas such as software, electrical, electronic, computational, and biomedical engineering, developed at a low cost, with easy access to the population, and non-invasive. However, when placed on evaluation, potential improvements were identified to increase the stability of Osseus operation.

Results

It is proposed the implementation of improvements in the antennas used by Osseus, aiming its miniaturization, improvement in the reception of the RF signal, and better stability of the equipment's operation.

Conclusion

Two antennas were then built, one of which was used as a project for the second, which is an array. The array showed significant improvements in the parameters relevant to the application, being a candidate to replace the antennas currently in use at Osseus.

Keywords:

Microstrip patch antenna, osteoporosis, biotelemetry, fracture, engineering, radio frequency.

Background

Applications of electromagnetic waves in the field of biotelemetry have increased in the latest years. Currently, these waves are used in the prevention, diagnosis, and treatment of a variety of diseases and play an important role in analysis and imaging, thermal therapies, administration of drugs and sensors^{1,2}. In this context, biotelemetry allows minimally invasive monitoring of physiological parameters, improving patient comfort and care and significantly reducing hospital costs^{3,4}.

The monitoring of physiological parameters can lead to the diagnosis and, consequently, to the early treatment of diseases, being essential for the implementation of preventive measures. Thus, in the case of osteoporosis, the risk of bone fractures can be reduced⁵.

Annually, millions of bone fractures resulting from osteoporosis happen worldwide. The most common bones with fracture incidence include those of the spine, forearm, proximal humerus, and hip⁶. Hip fractures are those with the highest morbidity and mortality and cause the highest direct costs to the health services, increasing exponentially when they affect the elderly population. It is estimated that in 2050 the number of hip fractures in men and women, within the range of 50 to 64 years in Latin America, will increase by 400%. In Brazil, ten million people, about one in seventeen, suffer from osteoporosis⁶.

To reduce costs with procedures for the treatment of bone fractures caused by osteoporosis, it is essential to implement preventive measures in view of the growing number of elderly people in Brazil and the worsening of the calamity that this disease has caused, hindering early detection and subsequent appropriate treatment⁷. In Brazil, the population has not been given adequate access to early diagnosis of the disease. One of the factors that lead to this is the complexity and high cost of the distribution of equipment throughout the Brazilian territory.

Based on what was exposed, in 2018, Osseus was proposed. An equipment capable of assisting in the classification of bone mineral density, by means of a radio frequency (RF) signal that would lead to a later diagnosis of osteoporosis. This instrument is a combination of the application of techniques and concepts from different areas such as software, electrical, electronic, computational, and biomedical engineering, developed at a low cost, with easy access to the population, and non-invasive⁶.

This procedure is done through the reading of a 2.45 GHz RF signal, which passes through the medial phalanx of a patient's middle finger, and, after the signal is received,

it is processed by a system that contains an embedded computational intelligence technique. Analyzing the intensity of the received RF signal, the system can provide a prognosis informing the necessity to refer or not the patient to perform an exam of bone densitometry.

Upon being put under evaluation, potential improvements were identified to increase the stability of the Osseus functioning. The intensity of the RF signal varied in the same patient for several measures, whether due to the positioning of the patient's finger between the antennas, or due to random factors. Another improvement of interest was the manufacturing of equipment with smaller dimensions, in order to increase its portability.

Thus, the physical configuration of the equipment was analyzed, as well as the antennas in use. Throughout the research, it was concluded that it was necessary for the pair of antennas used in the transmission/reception to be well-calibrated and to have very similar operating characteristics in terms of signal radiation.

In this scenario, microstrip antennas were a good alternative, as they are known for their miniaturization capacity and simplicity, and low manufacturing cost, despite their narrow bandwidth. However, bandwidth is not a relevant parameter for this application, as no information is being transmitted, but only an RF signal. Other parameters, such as impedance matching and directivity, are essential for the proper functioning of the device.

This article presents state-of-the-art microstrip antennas used in biotelemetry applications. Then we present the main improvements implemented in Osseus, the design of the proposed antennas to be used in the equipment, as well as the main results achieved.

Latest researches

The use of antennas in biomedical applications is vast, ranging from sensing to disease diagnosis. In the literature, there are countless researches with proposals for microstrip antennas, in biomedical applications. In this section, we try to identify the main publications in the last 4 years.

L. F. S. Moraes⁸ proposed a miniaturized double spiral antenna for implantable biomedical application at 2.41 GHz frequency band of the Industrial, Scientific, and Medical (ISM) band. Various antenna parameters such as return loss, impedance matching, gain, Voltage Standing Wave Ratio (VSWR), and radiation diagrams were carried. The proposed antenna is fed by the coplanar waveguide method. Only the return loss was measured, with no experimental evidence of other parameters. In addition, an antenna presented low purity of polarization and omnidirectional radiation.

M. Nachiappan and T. Azhagarsamy⁹ proposed broadband, low profile, and semi-flexible antenna for biomedical telemetry applications. The antenna was designed in a semi-flexible RT/duroid material. A conventional rectangular patch was modified by adding rectangular slits to reduce the resonance frequency and the ground plane was truncated and modified to increase the bandwidth. This antenna showed a gain close to the commercial ones, about 2.50 dBi at 2.4 GHz and high efficiency, about 93% at 2.4 GHz. Experimental results of the return loss, efficiency, gain, and radiation diagram were presented. Due to the truncation of the ground plane, the antenna showed omnidirectional radiation.

A. Smida et al¹⁰ proposed a triple-band microstrip antenna to operate on the frequencies of 434, 868, and 1400 MHz. The antenna is H-shaped and it was miniaturized, which made impedance matching difficult and significantly reduced its efficiency, falling below 3% in all operating frequencies. In addition, the antenna featured an omnidirectional diagram.

D. Nikolayev¹¹ proposed the design and analysis of miniaturized implantable conformable adhesive antennas for biomedical applications. A polyimide substrate material has been considered to achieve compliance. The proposed radiant element was a rectangular monopolar antenna with three split-ring resonators (SRR) and with coplanar waveguide (CPW) feed. The proposed antenna has an operating frequency of 2.41 GHz, with a bandwidth of 810 MHz and a gain of 2.62 dBi. The authors presented experimental results of the return loss and the radiation diagram.

K. N. Ketavath¹² proposed and designed a circularly polarized implantable broadband antenna operating in the 2.4 GHz ISM band for biomedical applications. Experimental results of the reflection coefficient and the axial ratio were presented. The fractional bandwidth and axial ratio were 5.45% and 5.69%, respectively.

Another circularly polarized antenna was proposed by Z-J. Yang¹³. The antenna operates in a double band, it is compact and loaded with a metamaterial (MTM), being suitable for biomedical applications. The proposed antenna system operates in the ISM band with central frequencies of 915 MHz (902–928 MHz) and 2450 MHz (2400–2480 MHz). The integration of the antenna with the metamaterial produced an improvement in the gain and behaved as a linear to circular polarization converter, in the two operating frequencies. The gains obtained were - 17dBi for 915 MHz and - 10dBi for 2450 MHz. The antenna presented an omnidirectional radiation diagram.

M. Zada¹⁴ proposed a clover-shaped split antenna operating in the 2.45 GHz ISM band, for biomedical applications. The proposal aimed at a miniaturized antenna with a wide bandwidth of 180 MHz. The antenna achieved a maximum gain of - 6 dBi. Results measured for the reflection coefficient and for the co-polarization and cross-polarization radiation diagrams were presented. The antenna showed omnidirectional radiation and a very low gain.

All of these researches have antennas with characteristics that do not match the requirements of Osseus, mainly because we need a directive antenna, with a Half Power Beam Width (HPBW) lower than 70° and with a gain greater than 2.5 dBi. In addition, the antenna has dimension restrictions due to the size of the equipment. Thus, in this research we propose an array of two-element microstrip antennas, to reduce the HPBW and provide a satisfactory gain, as well as occupying a reduced space.

Results

After the designing, the microstrip antenna and the microstrip antenna array, simulations of the main parameters of these antennas were performed in the commercial software ANSYS HFSS, as well as simulations for the Yagi antenna too. The purpose of these simulations is to compare the performance of the array with the other antennas.

Simulated results

The first parameter analyzed is the reflection coefficient. Figure 1 illustrates the simulated results for the three antennas. It can be seen that the Yagi antenna has a resonance frequency equal to 2.29 GHz and a bandwidth of 400 MHz. The patch antenna has a resonance frequency equal to 2.44 GHz and a bandwidth of 15 MHz. The antenna array has a resonance frequency of 2.45 GHz and a bandwidth of 25 MHz. The narrow bandwidth is not relevant to this application. Thus, we observed that the antenna array presents a good match of impedance and resonance frequency equal to that one of WiFi.

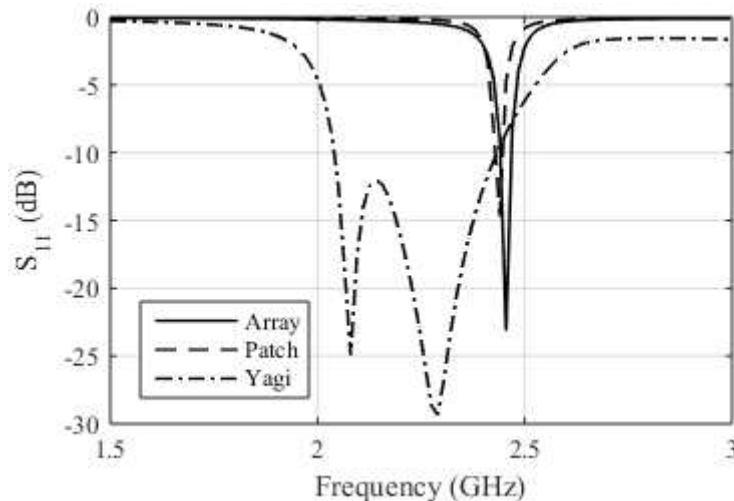
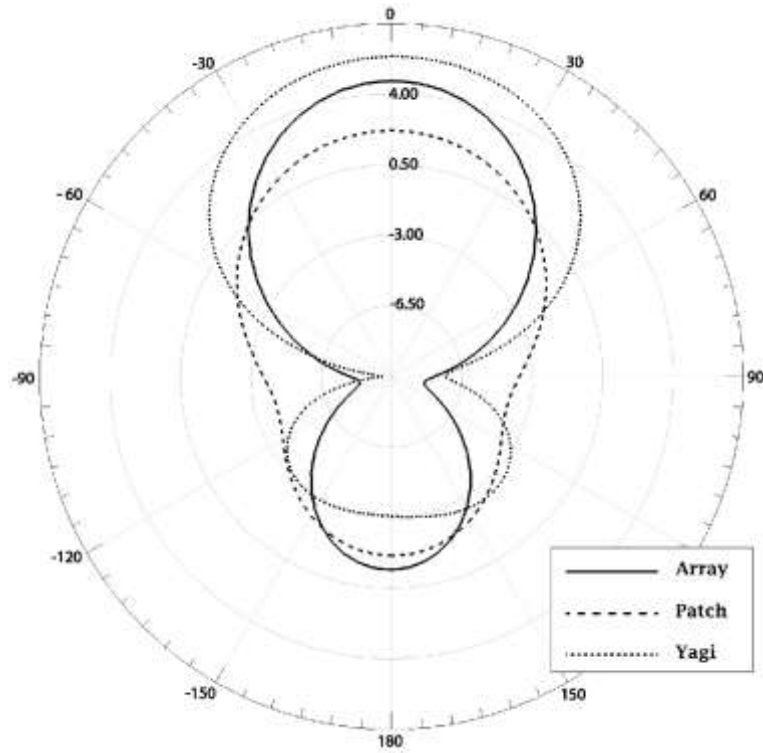


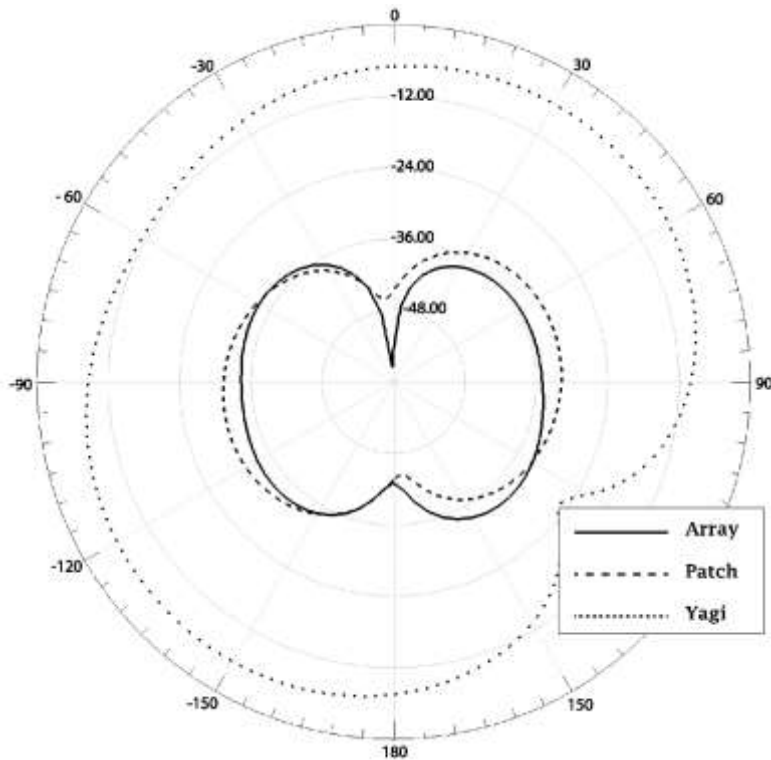
Figure 1 – Reflection coefficient for the three antennas analyzed.

Another important parameter that must be analyzed is the radiation diagram. This parameter was simulated for co-polarization and cross-polarization, which are illustrated in Figure 2. Figure 2(a) illustrates the simulated radiation diagrams for co-polarization. The Yagi antenna has the highest directivity, around 5.7 dBi, while the patch antenna has the lowest directivity, reaching around 2.5 dBi while the antenna array has 4.7 dBi. However, we can see that the antenna array has a better HPBW of 70°, while the patch antenna has 120° and the Yagi has 95°. Regarding the cross-polarization diagram, illustrated in Figure 2(b), we can notice that the Yagi antenna does not present polarization purity, with a difference of only 16 dB, comparing its co-polarization with

the cross-polarization. As for the antenna array, the cross-polarization level reached more than 40 dB below the co-polarization level, which shows a high polarization purity. The patch antenna also features high polarization purity, with a cross-polarization level of more than 35 dB below the co-polarization level.



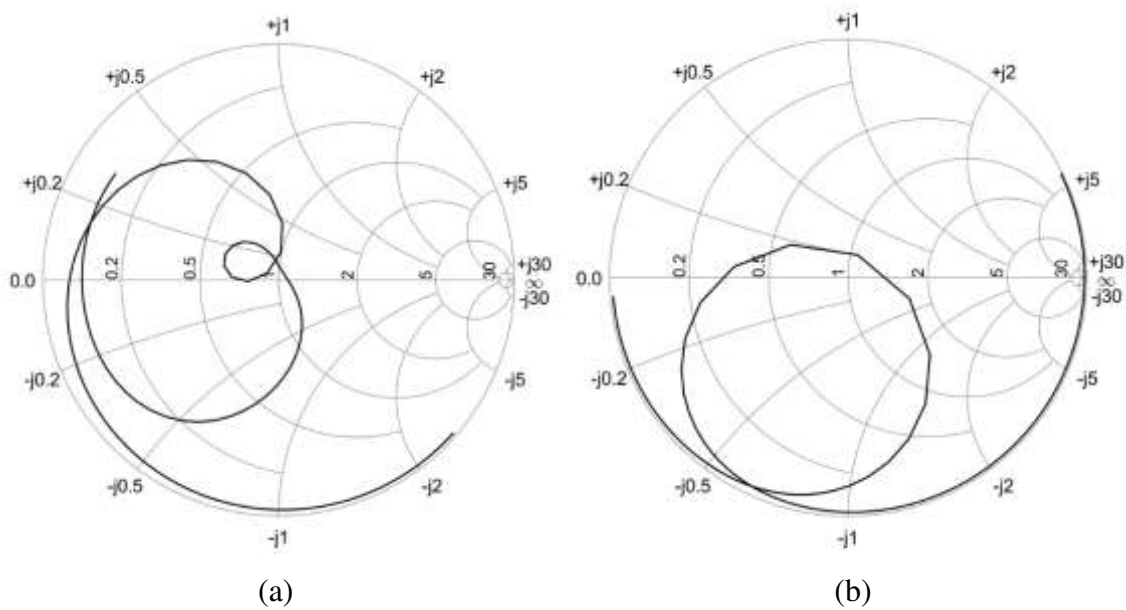
(a)



(b)

Figure 2 – Radiation diagrams: (a) co-polarization e (b) cross-polarization.

The next parameter to be analyzed is the Smith chart, which shows how the antenna impedance behaves as a function of the frequency. Figure 3 illustrates the Smith chart of the three antennas. For the Yagi antenna, the Smith chart is illustrated in Figure 3(a). It can be seen that the resonance occurs at 2.29 GHz and the normalized impedance was $1.065 + j 0.025 \Omega$. For the patch antenna, the resonance frequency occurs at approximately 2.45 GHz, but it can be seen in Figure 3(b) that the normalized impedance of the antenna does not cross the unit circle at this frequency, showing the need for improvement in the matching of antenna impedance. Finally, considering the antenna array, the resonance frequency occurs at approximately 2.45 GHz. The normalized impedance of the array crosses the unit circle, showing a good design of the feed network, with an input impedance of $49.5 - j7 \Omega$ (Figure 3(c)).



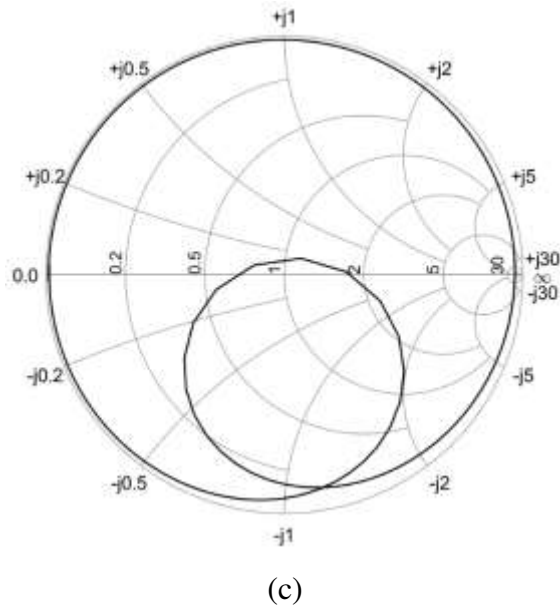


Figure 3 – Smith chart: (a) Yagi antenna, (b) Patch antenna and (c) Antenna array.

Table 1 shows the comparison between the Yagi antenna, patch antenna and antenna array, according to the parameters shown.

Table 1 – Parameters of the antennas analyzed for its resonance frequency.

Antenna	Parameter	Value
Yagi-Uda	Directivity	5.7 dBi
	Bandwidth	390 MHz
	Half power bandwidth (HPBW)	95°
	Front-to-back ratio	5.41 dB
Patch antenna	Directivity	2.52 dBi
	Bandwidth	16.3 MHz
	Half power bandwidth (HPBW)	120°
	Front-to-back ratio	3.3 dB
Antenna array	Directivity	4.7 dBi
	Bandwidth	25.4 MHz

	Half power bandwidth (HPBW)	70°
	Front-to-back ratio	5.1 dBi

Based on the data listed in Table 1, we can see that the antenna array has a lower performance than the antenna currently in use in Osseus, as the patch antenna too. However, the proposed array has smaller dimensions than the Yagi antenna used. While the array has dimensions of 3.5 cm × 7.0 cm, the Yagi antenna has dimensions of 6.6 cm × 7.0 cm. Both have equivalent performance in terms of directivity and front-to-back ratio. The antenna array has a lower bandwidth, but that is not relevant for the application. In addition, the array has a lower HPBW, which can promote better results and an improvement in equipment performance, since stability is an issue. Finally, the way in which the coaxial cable is connected to the antenna array eliminates the instabilities found in the Yagi, which can prove to be a significant improvement. Another fact to be noted is that the Yagi antenna is positioned along the longest axis of the Osseus equipment, while the antenna array will be placed perpendicular to that axis. In this way, the antennas will operate in the distant field region. This will prevent variations in the reading of the signal intensity from occurring.

From the decision of the antenna that would be used in the equipment, some prototypes were manufactured for experimental validation and to analyze the improvements in the equipment. Figure 4 illustrates the Yagi antenna currently in use compared in scale to the built antenna array.

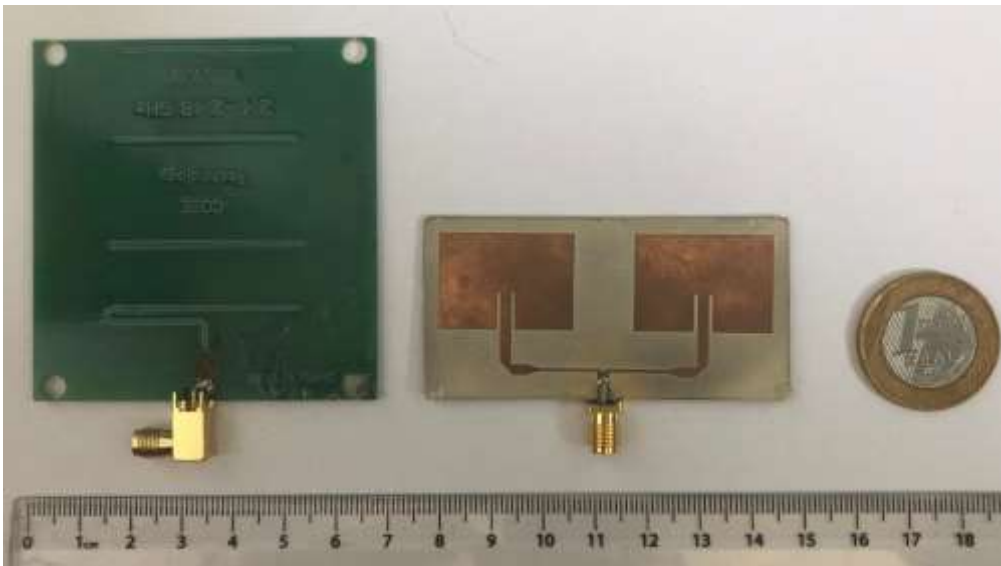


Figure 4 – Yagi antenna currently in use compared in scale to the antenna array.

Measured results

The measurement setup was set up with various equipment. The Agilent two-port network vector analyzer, model E5071C, with a measurement range from 300 KHz to 14 GHz was used. Cables appropriate for this frequency range were used. In addition, for gain measurement, we used standard horn antennas model SAS-571 (double ridge guide horn antennas). We tried to measure all possible parameters, with the available setup. The parameters measured were: the modulus of the reflection coefficient ($|S_{11}|$), gain of the array, and the Smith chart.

The first parameter measured was S_{11} , which allows us to analyze the resonance frequency of the antenna and its bandwidth. We measured this parameter for four manufactured arrays. Figure 5 illustrates this parameter. We can see that the antennas responded in a similar way. The antenna arrays that presented the best impedance matching were installed in Osseus. Figure 6 illustrates the frequency response of S_{11} only for these two arrays. We can see that the results are very similar.

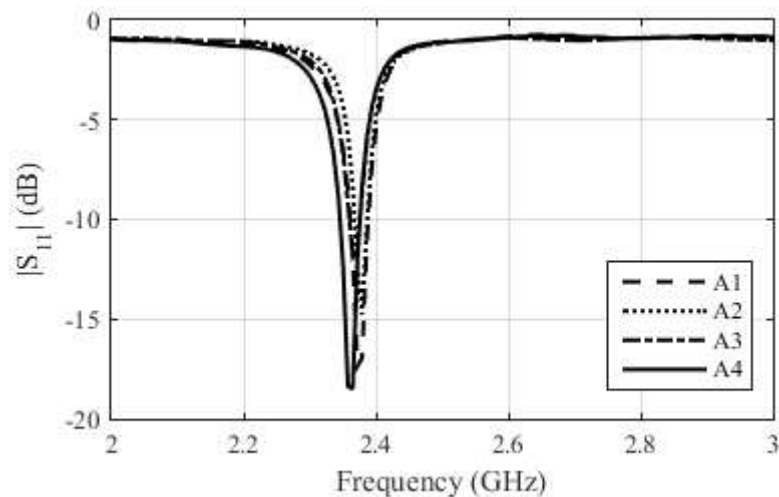


Figure 5 – S_{11} measure for the four constructed antenna arrays.

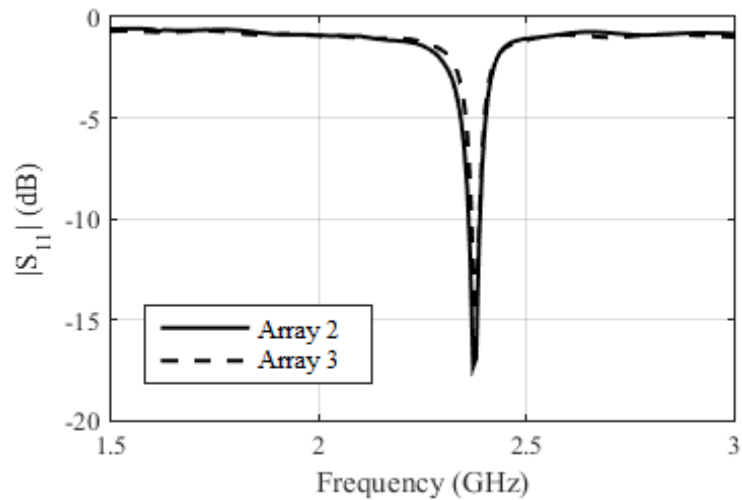


Figure 6 – S_{11} for the antenna arrays 2 and 3 constructed.

In Figure 7, we compared the simulated S_{11} with the measured response for antenna array 2. We can see that there was a small difference between the results. This is perhaps due to the manufacturing process, which was not done with a milling machine. This difference is not a problem, as *Osseus* has a voltage-controlled oscillator, whose oscillation frequency can be regulated between 2.25 and 2.65 GHz.

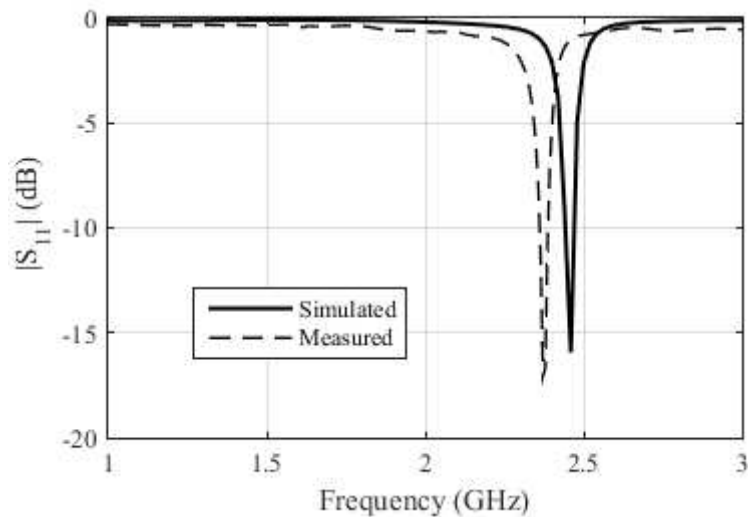


Figure 7 – Comparison between the simulated and measured S_{11} for antenna array 2.

Figure 8 illustrates the measured Smith chart. We can see a reactance greater than that obtained in the simulation, which was 7Ω , while the measured value was 12Ω . This difference represented in the reactance caused a reduction in the resonance frequency.

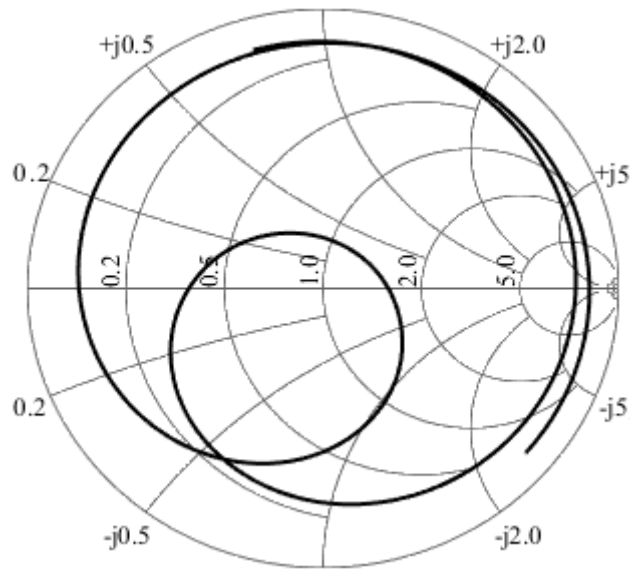


Figure 8 – Smith chart for constructed antenna array 2.

Figure 9 shows the comparison between the simulated and measured gains for the antenna array 2, near to the value of maximum gain.

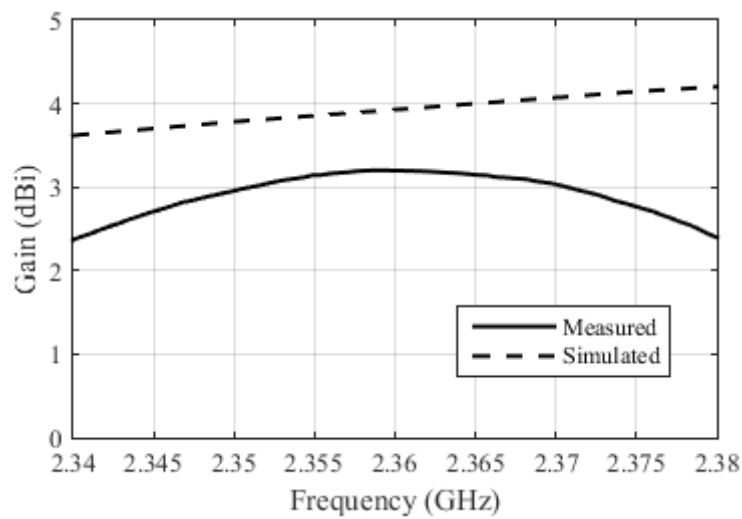


Figure 9 – Comparison between the simulated and measured gains for the constructed antenna array 2.

Discussion

One of the main improvements that needed to be made in Osseus was to reduce possible variations in the reading of the signal intensity. It is important that the signal-to-noise ratio (SNR) received remains constant, or that it undergoes minimal changes. This will allow computational intelligence tools to achieve a more accurate classification when doing the screening. It is observed that the previous version of the Osseus, with the Yagi-

Uda antennas, presented considerable SNR variations, depending on the position of the finger inserted in the equipment. To perform the measurements, two positions of the finger were considered, as shown in Figure 10. The first measurement is made with the finger inserted in the position considered correct (Figure 10(a)) and the second measurement is made with the finger inserted in the position considered rotated (Figure 10(b)). This will cause the RF signal to reach a greater or lesser finger surface. The desired result is that the SNR does not vary, even with the finger inserted in a rotated manner, allowing a more stable reading.



(a)

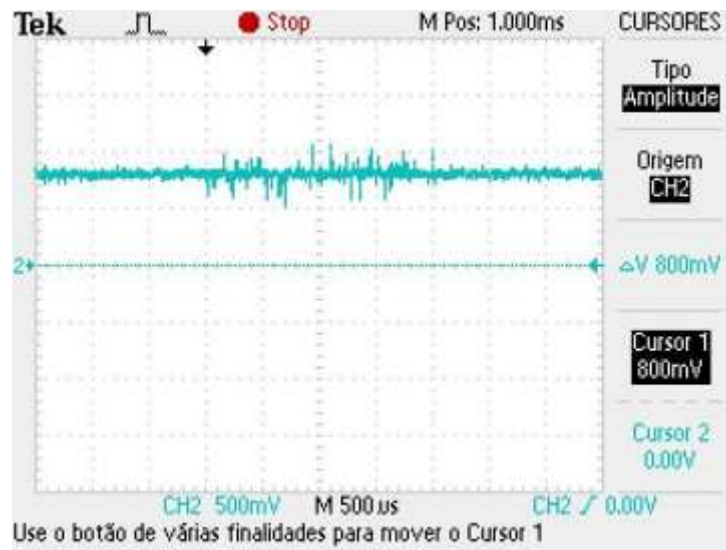


(b)

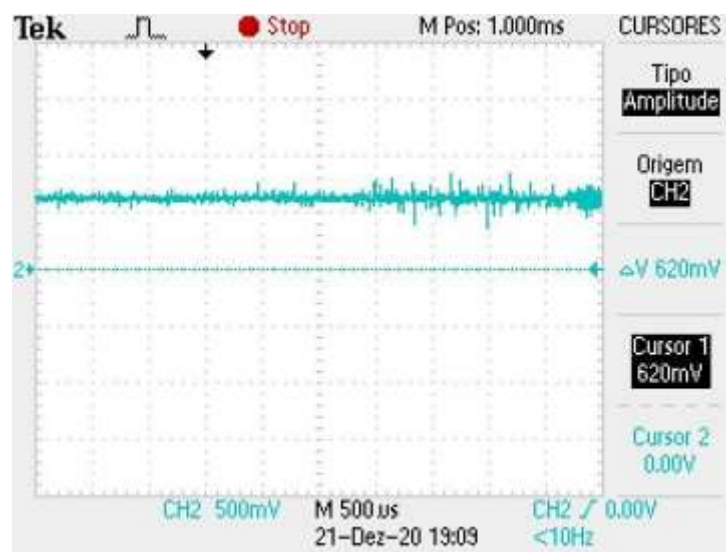
Figure 10 - Insertion of middle finger in positions: (a) correct and (b) rotated.

The received signal is obtained in a form of a level of direct current (DC) with a certain level of background noise coupled to it. The DC signal has a maximum level when there is no obstacle between the antennas and this value gets lower when the finger is inserted into the equipment. Also, a shield made with absorbers was inserted inside the box, so that the noise level remains constant, regardless of the reading, with or without the finger. Figure 11(a) illustrates the DC level received for a direct reading (without the

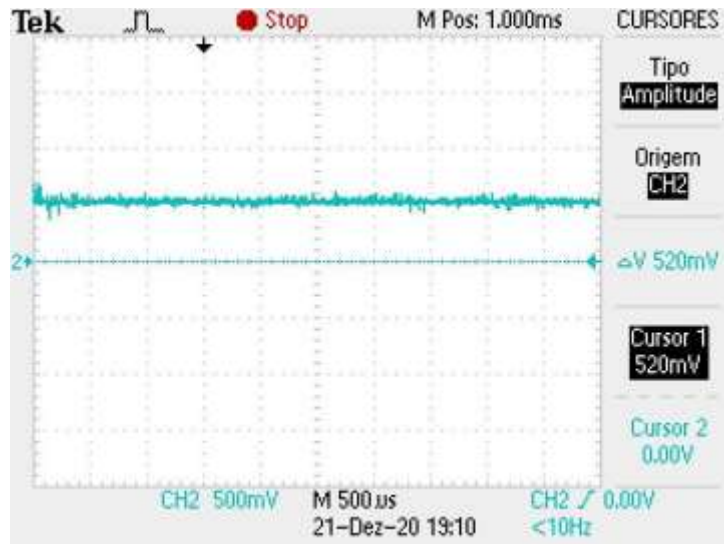
finger insertion), for the case of the first version of Osseus, with the Yagi-Uda antennas. In Figures 11(b) and (c) we can see the readings with the finger insertion in the correct and rotated position, respectively. It can be seen that there is a considerable level of noise, in addition to noticing a variation in the level of the received signal, for the different positions of the finger. Without the finger, the received signal is about 800 mV. For the reading with the finger in the correct position, the received signal is 620 mV, while for the reading with the finger in the rotated position, the received signal is 520 mV. In the frequency domain, we can verify whether the noise varies or not. Thus, the same measurements were made and the results can be seen in Figure 12. The noise level for the three situations considered above was - 61.4 dB, with no variation for the situations with or without the finger.



(a)

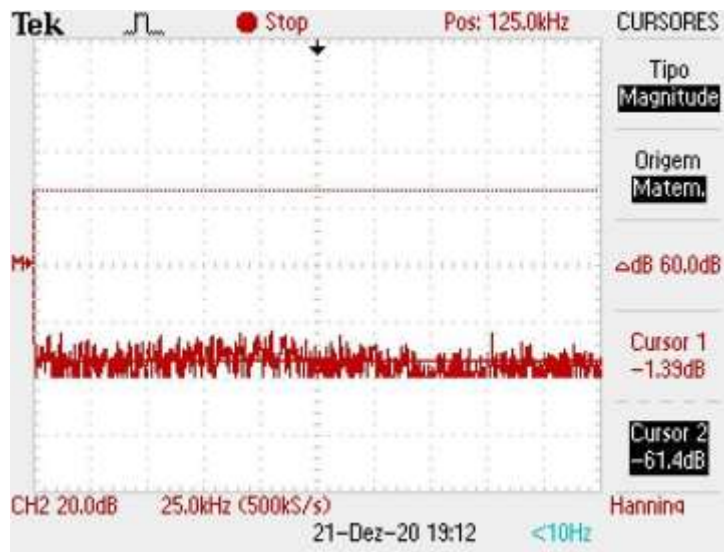


(b)

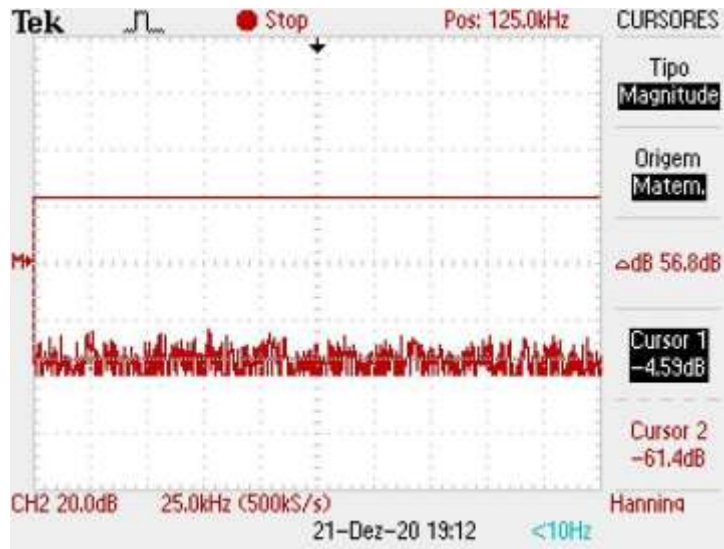


(c)

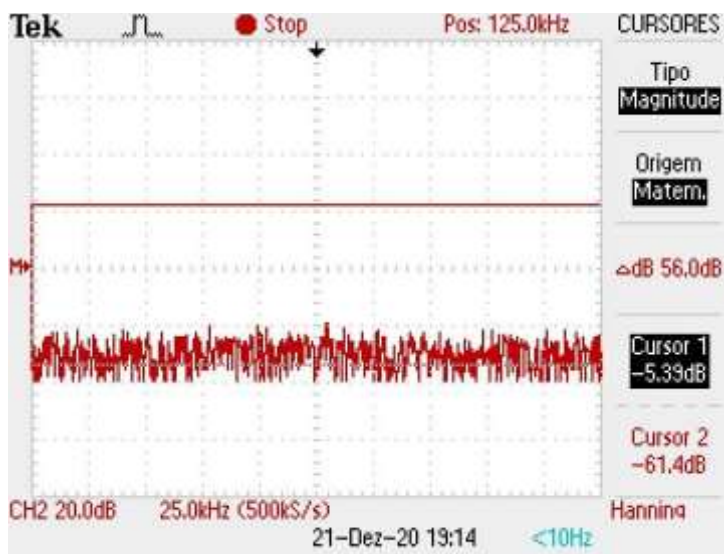
Figure 11 - Reading of the DC level of the received signal for the first version of the *Osseus*: (a) without finger, (b) with finger in the correct decision e (c) with the finger in the rotated position.



(a)



(b)



(c)

Figure 12 -Reading of the noise level in frequency domain for the first version of the *Osseus*: (a) without finger, (b) with finger in the correct decision e (c) with the finger in the rotated position.

The same measurements were made for the second version of *Osseus*, with the antenna array. Figure 13(a) illustrates the DC level received for reading without the finger and in Figures 13(b) and (c) we have the readings with the finger inserted in the correct and rotated position, respectively. It can be seen that the noise level has decreased considerably, in addition to the fact that we no longer have a variation in the level of the received signal, for the different positions of the finger. The received signal intensity was also higher. Without the finger, the received signal was 1.70 V. For the reading with the finger in the correct and rotated positions, the received signal was 1.34 V. In the frequency

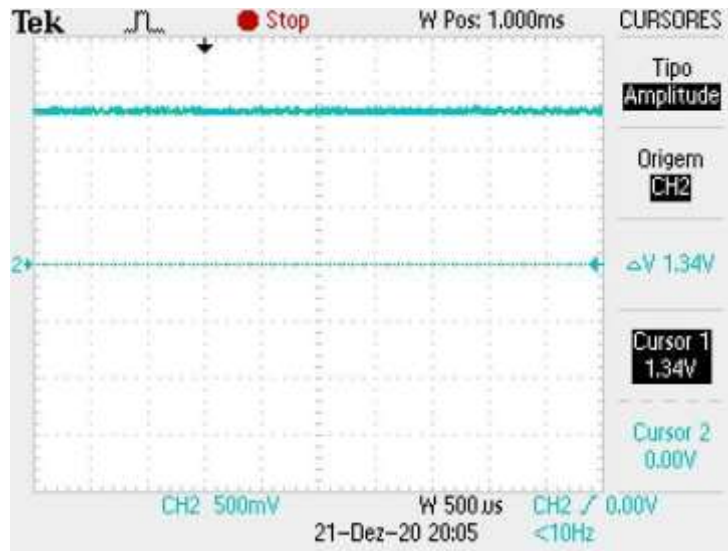
domain, we can verify that the noise did not varied. Thus, the same measures were made and the results can be seen in Figure 14. The noise level for the three situations considered above was - 64.6 dB, a reduction of 3.2 dB, compared to the first version of Osseus.



(a)



(b)

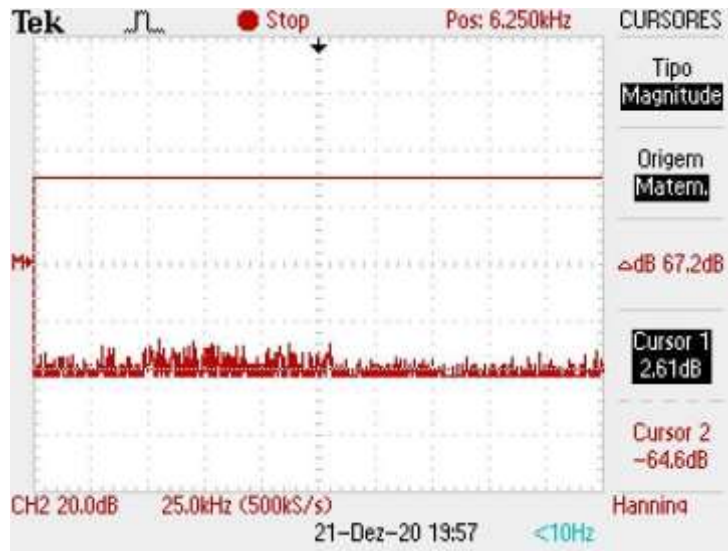


(c)

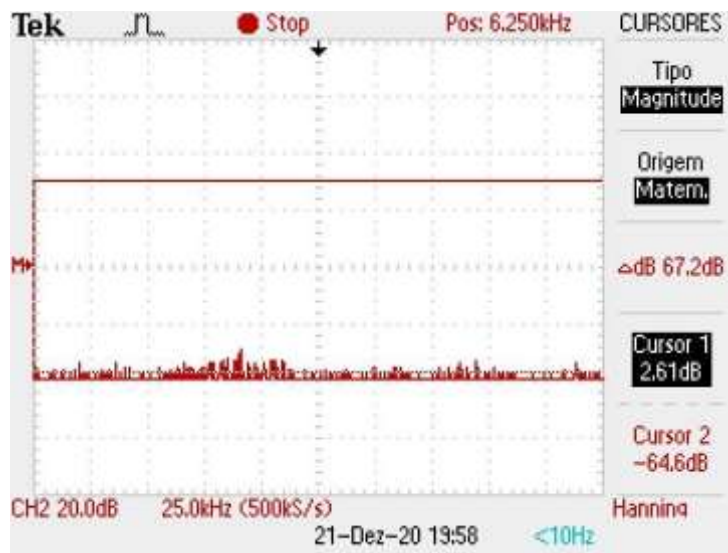
Figure 13 - Reading of the DC level of the received signal for the second version of the *Osseus*: (a) without finger, (b) with finger in the correct decision e (c) with the finger in the rotated position.



(a)



(b)



(c)

Figure 14 - Reading of the noise level in frequency domain for the second version of the *Osseus*: (a) without finger, (b) with finger in the correct decision e (c) with the finger in the rotated position.

Based on the measurements made, it was possible to obtain the signal-to-noise ratio for all situations considered, for both versions of the equipment. Table 2 illustrates the SNR values obtained for each situation considered. We can observe an increase of more than 8 dB in the SNR, in all situations, which represents a very significant improvement.

Table 2 - Measurements of SNR for the two versions of *Osseus*.

Version of <i>Osseus</i>	Situation	SNR measured
--------------------------	-----------	--------------

First	without the finger	26.03 dB
	with finger in correct position	24.66 dB
	with finger in rotated position	23.32 dB
Second	without the finger	34.83 dB
	with finger in correct position	33.22 dB
	with finger in rotated position	33.22 dB

Conclusions

The antennas currently in use in Osseus were characterized, to find out if they were the most appropriate for the equipment. The main parameters of the antenna were simulated in the HFSS software. It was observed that there is no uniformity of these parameters within the entire operating range. The antenna showed a satisfactory gain in the resonance frequency, but this gain suffered a great variation throughout the operating range. In addition, the HPBW of the antenna proved to be high.

A new antenna configuration was proposed, aiming to improve some performance parameters, such as directivity and HPBW. For this, it was proposed to design an antenna to replace the current antenna used in Osseus. The results of a simple rectangular patch antenna with inset fed were shown. In addition, an antenna array was designed with two microstrip patch antennas, identical to the first designed antenna. It was noticed that the array has a performance similar to that of the antenna currently in use in OSSEUS. However, the array has a lower HPBW and smaller dimensions when compared to the Yagi antenna. The kind of array designed reduces the problem of connecting the coaxial cable to the antenna. The main parameters of the antenna and array were simulated in the HFSS software. Four prototypes of the proposed antenna array were built, aiming at tests on the Osseus equipment, as well as the measurement of the antenna parameters, such as S_{11} , gain, and Smith chart.

The measurements showed that the prototypes of the antenna arrays constructed showed similar performances, regarding the measured parameters. We selected the two best arrays to be installed in *Osseus*

With the insertion of new antennas and a reduction in the size of the Osseus box, significant improvements in the intensity of the received signal, in the noise level, and in the signal-to-noise ratio were observed. SNR increased by more than 8dB. These improvements will allow for more accurate classification of the equipment.

Methods

The first part of the research aimed to identify possible improvements in *Osseus*. Thus, characterizing the antennas used previously was an important action to start up this task. The antenna used a Yagi type, which is a directive antenna, with a gain of approximately 4 dBi. The input impedance of the antenna is 50Ω , which allows easy matching for most of the feed networks.

The Yagi antenna is illustrated in Figure 15. It has a 50Ω single-ended feed input and this transmission line is converted into a two-wire feed through the conductive path.

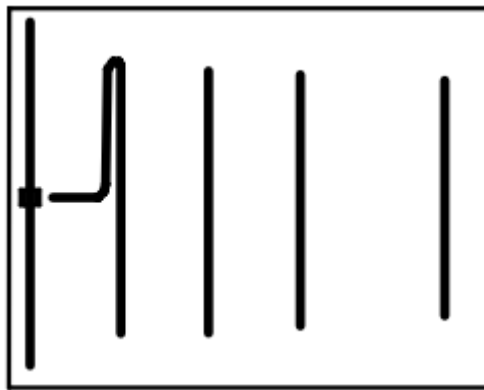


Figure 15 – Yagi-Uda antenna analyzed.

One of the main problems of this antenna is the way that the coaxial cable is connected to it. Figure 16 illustrates this form of connection. It can be seen that a minimum error in welding can lead to an impedance mismatch changing the way it operates. The ground mesh must be welded on the reflector part and the central conductor of the coaxial cable must be welded on the dipole.

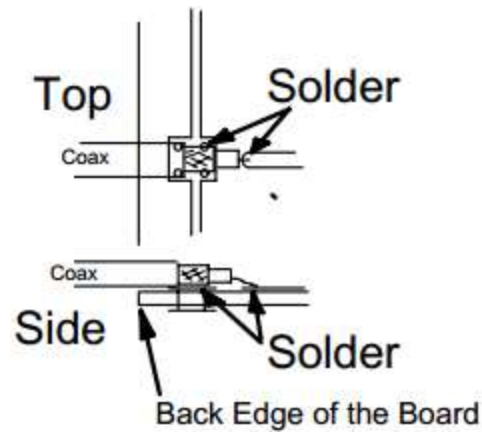


Figure 16 – Connection between the coaxial cable and the Yagi-Uda antenna analyzed.

Another problem refers to the region in which the electromagnetic field of this application is located. This type of antenna must operate in the distant field region, that is, the two antennas must be separated by a distance of $2R$, where R is calculated as:

$$R > \frac{2D^2}{\lambda} \quad (1)$$

In which D is the largest linear dimension of the antenna and λ is the wavelength of the antenna's resonance frequency.

This field regions are illustrated in Figure 17.

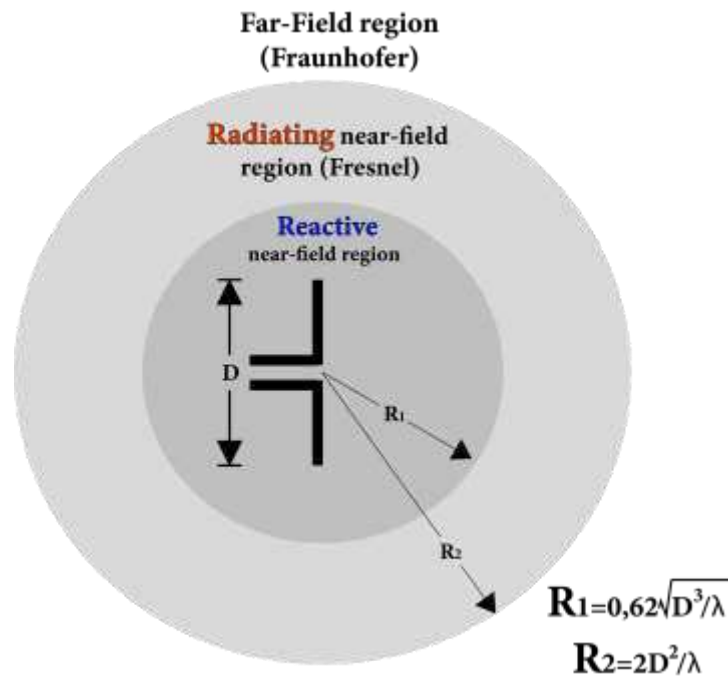


Figure 17 – Near field and far field regions.

For this Yagi antenna, the dimension D is 63 mm and λ is 122.45 mm. Thus, the distant field region starts at approximately 65 mm, which indicates that the antennas should be separated by a distance greater than about 130 mm, at least. Nonetheless, due to a volume restriction of the equipment, the antennas were separated by less than 30 mm, which would make them operate in the near field region, which could lead to erroneous readings of the signal intensity.

Finally, we must have an antenna whose HPBW is the smallest possible, for this application, aiming to concentrate the RF signal as much as possible. It is worth mentioning that the total volume of the equipment limits this factor, as it does not allow us to have highly directive arrays, with many elements. The analyzed Yagi antenna has a 95° HPBW.

Thus, we conclude that the Yagi antenna was not suitable for use in *Osseus*, and another antenna, or an array of antennas, had to be proposed to meet all the criteria listed in this section.

Project of the antenna and antenna array

From what was exposed in the previous section, we listed some parameters of the antenna in use to be improved. The antenna needs to be as small as possible to meet the portable device's final volume requirements. The antenna feed must be done in a more consistent way, via SMA connector soldered to it. The antenna needs an improvement in the gain, directivity, and, consequently, in the reduction of the HPBW. To guarantee certain radiation parameters, the antenna needs good impedance matching, along with a consistent way to input the signal of 2.45 GHz.

Based on the issues that need to be improved, a microstrip patch antenna and a patch antenna array have been proposed. As an initial proposal, we will start with a simple concept of a planar microstrip antenna with rectangular patch geometry. Unlike the initial antenna, this antenna has a ground plane completely filled over the entire length of the dielectric. The chosen feed was via a microstrip line and the impedance matching with the input is made by inserting a line gap in the rectangular patch (Inset Fed). An illustration of this model can be seen in Figure 18.

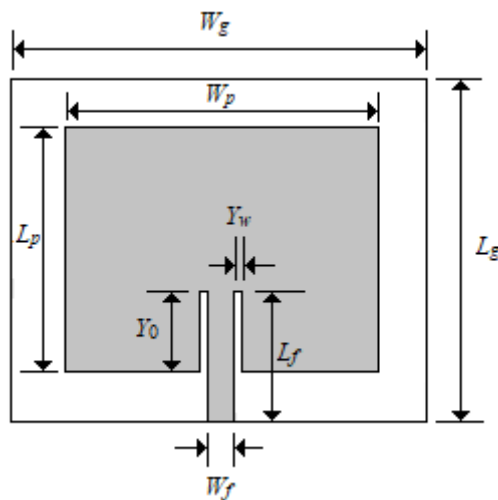


Figura 18 – Antena patch de microfita.

For the design of this type of antenna, the classic approach presented by S. A. Kumar and T. Shanmuganatham¹⁵ was used, which systematically describes how to design this kind of geometry. It is important to choose the appropriate dielectric material. In this approach, it is evident that the physical dimensions of the antenna can be reduced if we use a dielectric material with high relative electrical permittivity. Thus, the *ROGERS RO3010* was chosen, with $\epsilon_r = 10.2$ and thickness $h = 1.27$ mm. The increase in ϵ_r tends

to reduce the bandwidth, so we choose the largest thickness available from this manufacturer, compensating for this reduction¹⁵.

Initially, the dimensions of the rectangular patch¹⁵ are determined as:

$$W = \frac{c}{2f_r} \sqrt{\frac{2}{\epsilon_r + 1}} \quad (2)$$

$$L = \frac{c}{2f_r \sqrt{\epsilon_{eff}}} + 2\Delta L \quad (3)$$

In which,

$$\epsilon_{eff} = \frac{\epsilon_r + 1}{2} + \frac{\epsilon_r - 1}{2} \left[1 + 12 \frac{h}{W} \right]^{-\frac{1}{2}} \quad \text{for } \frac{W}{h} > 1 \quad (4)$$

$$\frac{\Delta L}{h} = 0,412 \frac{(\epsilon_{eff} + 0,3) \left(\frac{W}{h} + 0,264 \right)}{(\epsilon_{eff} - 0,258) \left(\frac{W}{h} + 0,8 \right)} \quad (5)$$

Besides that, c is the speed of light in the vacuum, f_r is the desired resonance frequency, ϵ_{eff} is the effective permittivity of the dielectric, and ΔL is the extended electrical length of the rectangular patch, due to the fringe effect¹⁶.

The next step is to design the gap in the patch, which will be responsible for the impedance matching for the antenna with its microstrip feed line. To do this, we need to calculate the patch impedance:

$$G_1 = \frac{1}{90} \left(\frac{W}{\lambda_0} \right)^2 \quad \text{for } W \ll \lambda_0 \quad (6)$$

$$R_{in} = \frac{1}{2G_1} \quad (7)$$

$$R_{in}(y = y_0) = R_{in} \left(\frac{\pi}{L} y_0 \right) \quad (8)$$

where G_1 is the approximate conductance of one of the patch slots, R_{in} is the approximate resistance of the patch, $R_{in}(y = y_0)$ is the resistance of the patch after the insertion of the gaps and y_0 is the length of the gap.

The width of the gap (Y_w) can be approximated by a quarter of the width of the microfiche line (W_f) that feeds the patch. According to the literature, this value usually

brings a good impedance match. Therefore, by finding the approximate impedance of the patch and making the resulting impedance 50Ω , for a correct match with the line of the same impedance, we project the inset fed.

Finally, we still need to design the microstrip line that will feed the patch. It should have a total length of an odd multiple of $\lambda/4$ and a width that results in an impedance of 50Ω :

$$Z_{intha} = \sqrt{\epsilon_{eff}} \left[\frac{W_0}{h} + 1,393 + 0,667 \ln \ln \left(\frac{W_0}{h} + 1,444 \right) \right] \quad (9)$$

Thus, using the expressions above, the physical dimensions for the antenna are listed in Table 3.

Table 3 – Dimensions of the antenna, microstrip line and *inset fed* (in mm).

<i>Patch</i>	W_p	25.8
	L_p	18.8
Entire dielectric	W_g	30.0
	L_g	30.0
Microstrip line	L_f	16.8
	W_f	2.0
<i>Inset-fed</i>	Y_w	0.8
	Y_0	8.0

The proposed array is illustrated in Figure 19. In this case, the impedance matching will not be done by an inset fed, but by a network feed, whose physical dimensions are determined from the desired impedance values. The elements of the array are identical to the rectangular patch antenna.

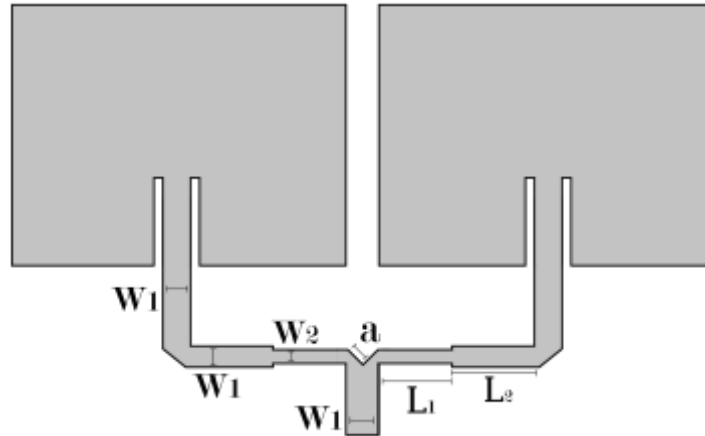


Figure 19 – Antenna array and its proposed network feed.

The literature shows us that an array has as its basic characteristic an improvement in directivity and, consequently, the maximum gain along with the reduction of the HPBW, which are the parameters that we want to improve. Therefore, the design of the parallel array comes down to create a network feed that injects the signal in an equivalent way for two identical patches. This network feed must have a good impedance matching between each of its steps, to ensure that the injected signal reaches the radiator elements with the least possible loss^{17,18}.

Initially, it is necessary to design a power divider. There are many different models of power dividers, but the T-type junction was chosen for ease of design and manufacture. This junction can be seen in Figure 20 and will serve to equally divide the power of the injected signal. In the T-junction, the impedance of each line determines its width, and the “V” shape with dimension “a” is necessary to minimize the parasitic reactances that arise due to the discontinuity of this junction.

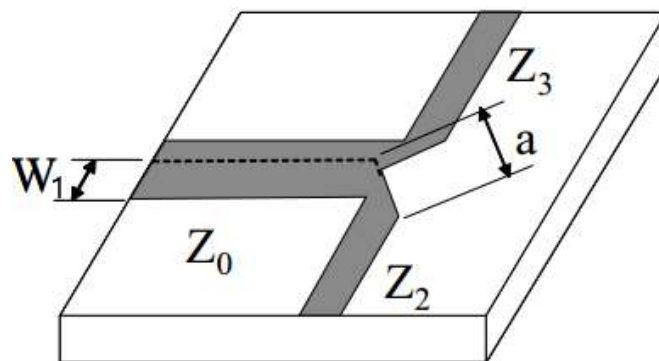


Figure 20 – T-type junction.

In Visser¹⁷, it is recommended for “a” to be $1.8W_1$. Whenever there is a discontinuity the same rule will be applied. It is important to note that if we want to divide

the signal intensity equally for both antennas, we need the junction lines to have twice the impedance of the line that receives the power. We can verify this through the following expressions:

$$P_1 = P_2 + P_3 \quad (10)$$

$$P_2 = \frac{1}{1 + K^2} P_1 \quad (11)$$

$$P_3 = \frac{K^2}{1 + K^2} P_1 \quad (12)$$

$$\frac{Z_2}{Z_3} = \frac{P_2}{P_3} = K^2 \quad (13)$$

$$\frac{Z_2}{Z_0} = \frac{P_1}{P_2} = 1 + K^2 \quad (14)$$

$$Z_2 = (1 + K^2)Z_0 \quad (15)$$

$$Z_3 = \left(\frac{1 + K^2}{K^2}\right)Z_0 \quad (16)$$

In which:

P_1 is the power delivered to the array;

P_2 is the power delivered to one of the elements of the array;

P_3 is the power delivered to the other element of the array;

K is a factor that determines the proportion how the power will be divided ($K=1$ for equal division of power);

Z_0 is the characteristic impedance of the feed line;

Z_2 is the impedance of one of the sides of the T-junction;

Z_3 is the impedance of the other side of the T-junction.

As the lines that follow from the T-junction have an impedance different than 50Ω , it is necessary to use an impedance transformer so that the network feed is matched with the antennas that we initially designed. The transformer used will be the one-quarter wavelength transformer. Its width is determined from the desired impedance, that is 50Ω . Figure 21 illustrates the insertion of the $\lambda/4$ transformer.

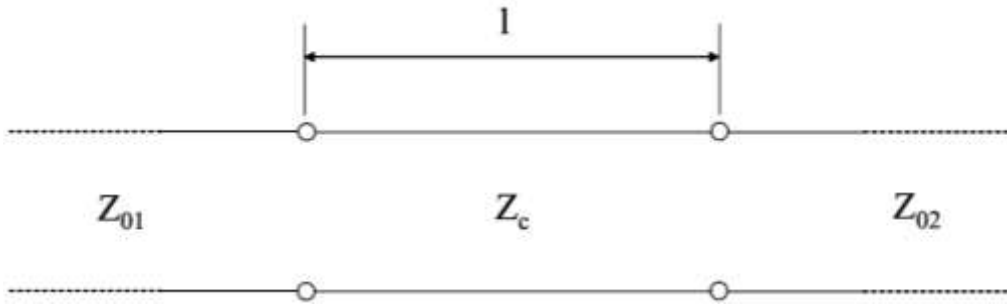


Figure 21 –Insertion of $\lambda/4$ transformer.

To calculate the dimensions of the transformer, we consider the length $\lambda/4$ and the width obtained from (9), knowing that the impedance of the transformer must be:

$$Z_c = \sqrt{Z_{01}Z_{02}} \quad (17)$$

In which Z_{01} is the impedance of the line of the T-junction and Z_{02} is the impedance of the antenna.

In this way, we completed the design of the array's network feed by obtaining all of its physical dimensions. Lesser adjustments will need to be made, due to the fact that some of the expressions are approximate and, mainly, due to the fact that the high permittiveness we use to reduce the dimensions of the antenna causes a greater fringe effect.

Table 4 lists the dimensions of the network feed for this antenna array.

Table 4 – Dimensions of the network feed of the array (in mm).

Dimension	measure in mm
L_2	12.2
L_3	5.6
W_1	2.0
W_2	0.55
W_3	2.0
a	1.0

References

1. A. Rosen, M. A. Stuchly, and A. Vander Vorst, "Applications of RF/microwaves in medicine," *IEEE Trans. Microw. Theory Tech.*, vol. 50, no. 3, pp. 963–974, 2002.
2. D. Kissinger and J.-C. Chiao, "Medical Applications of Radio-Frequency and Microwaves Sensing, Monitoring, and Diagnostics [From the Guest Editors' Desk]," *IEEE Microw. Mag.*, vol. 16, no. 4, pp. 34–38, May 2015.
3. K. S. Nikita, *Handbook of Biomedical Telemetry*. John Wiley & Sons, 2014.
4. A. S. Cruz, H. C. Lins, R. V. A. Medeiros, J. M. F. Filho, and S. G. da Silva.
5. "Artificial intelligence on the identification of risk groups for osteoporosis, a general review", *BioMedical Engineering OnLine*, vol. 17, no. 1, pp 1 – 17, 2018.
6. A. S. Cruz, "Osseus – Método baseado em inteligência artificial e ondas eletromagnéticas para o diagnóstico auxiliar de doenças osteometabólicas" (in Portuguese), PhD Thesis, Universidade Federal do Rio Grande do Norte, Brazil, 2018.
7. D. V. Araújo, J. H. A. de Oliveira, and O. L. Bracco, "Custo da fratura osteoporótica de fêmur no sistema suplementar de saúde brasileiro" (in Portuguese), *Arquivos Brasileiros de Endocrinologia & Metabologia*, vol. 49 no. 6, pp 897 – 901, 2005.
8. L. F. S. Moraes, "Gastos do ministério da saúde e estimativa de idosos com osteoporose tratados no sistema Único de saúde do brasil no triênio 2008-2010" (in Portuguese), Master Thesis, Universidade de Brasília Faculdade de Ciências da Saúde, Brasília, DF, Brazil, 2014.
9. M. Nachiappan and T. Azhagarsamy, "Design and development of dual-spiral antenna for implantable biomedical applications", *Biomedical Research*, vol. 28, no. 12, pp 5237 - 5240, 2017.
10. A. Smida et al., "Wideband Wearable Antenna for Biomedical Telemetry Applications", *IEEE Access*, Vol. 8, 2020, pp. 15687 - 15694.
11. D. Nikolayev, W. Joseph, A. Skrivervik, et al., "Dielectric-Loaded Conformal Microstrip Antennas for Versatile In-Body Applications", *IEEE Antennas and Wireless Propagation Letters*, Vol. 18, no. 12, pp. 2686 - 2690, 2019.

12. K. N. Ketavath, D. Gopi, and S. S. Rani, "In-Vitro Test of Miniaturized CPW-Fed Implantable Conformal Patch Antenna at ISM Band for Biomedical Applications", IEEE Access, Vol. 7, pp. 43547 - 43554, 2019.
13. Z-J. Yang, S-Q. Xiao, L. Zhu, B-Z. Wang, and H-L. Tu, "A Circularly Polarized Implantable Antenna for 2.4-GHz ISM Band Biomedical Applications", 2554 IEEE Antennas and Wireless Propagation Letters, Vol. 16, pp. 2554 - 2557, 2017.
14. M. Zada, I. A. Shah, and H. Yoo, "Metamaterial-Loaded Compact High-Gain Dual-Band Circularly Polarized Implantable Antenna System for Multiple Biomedical Applications."
15. S. A. Kumar and T. Shanmuganatham, "Design of clover slot antenna for biomedical applications", Alexandria Engineering Journal (2017) 56, 313–317. Biomedical Applications", IEEE Transactions on Antennas and Propagation, Vol. 68, no. 2, pp. 1140 - 1144, 2020.
16. Balanis, C., "Teoria de antenas: Análise e síntese", Livros Técnicos e Científicos, 2008.
17. RO3010 Laminates, available in:
<https://www.rogerscorp.com/acs/products/39/RO3006-and-RO3010-Laminates.aspx>, accessed in 07/12/2019.
18. Visser, H. J., "Array and Phased Array Antenna Basics 1st Edition", Wiley, 2005.
19. Pozar, D. M., "Microwave Engineering", Wiley, 2011.

List of abbreviations

RF - Radio Frequency.

ISM - Industrial, Scientific, and Medical.

SRR - Split-Ring Resonators.

CPW - Coplanar Waveguide.

MTM – Metamaterial.

HPBW - Half Power Beam Width.

SNR - Signal-to-Noise Ratio.

DC - Direct Current.

mm – millimeters.

mV - miliVolts.

V - Volts.

KHz - KiloHertz.

MHz - MegaHertz.

GHz - GigaHertz.

dB - Decibels.

dBi - Decibels Isotropic.

VSWR - Voltage Standing Wave Ratio.

Wifi - Wireless Fidelity.

SMA – Sub Miniature Version A.

Declarations

- Ethics approval and consent to participate:

Not applicable.

- Consent for publication:

Not applicable.

- Availability of data and materials:

The datasets during and/or analyzed during the current study available from the corresponding author on reasonable request.

- Competing interests:

The authors declare that they have no competing interests.

- Funding:

The research that led to the writing of this manuscript is funded by the Ministry of Health of Brazil

- Authors' contributions:

ASC started the research that gave rise to this work, developing the first versions of Osseus and carrying out the first tests with built prototypes. In this manuscript he was also responsible for revising and writing part of the introduction.

BMP, as main author, carried out the research base, as a doctoral student. He designed, simulated, built and measured all the antennas mentioned in the manuscript. Participated in the writing of the entire text and performed the translation into English and also participated in the review of the manuscript.

ALPSC, as BMP's academic advisor, he actively participated in all stages of research and writing of this manuscript, guiding the main author before writing and revising after writing.

DDAC was responsible for all of electronic instrumentation necessary for the verification of the antennas mentioned in the manuscript, carrying out the construction of a new prototype of Osseus and making use of it for the laboratory testing of the new antennas, the old antennas and the comparison between them.

RAMV participated as an advisor for this and all other research related to Osseus, leading a total of six teams for writing manuscripts in several areas that make up Osseus..

NVRV participated in the manuscript review meetings suggesting several improvements in the writing construction phase.

JPQS participated in the manuscript review meetings suggesting several improvements in the writing construction phase.

All authors read and approved the final manuscript.

- Acknowledgements

Not applicable.

Figures

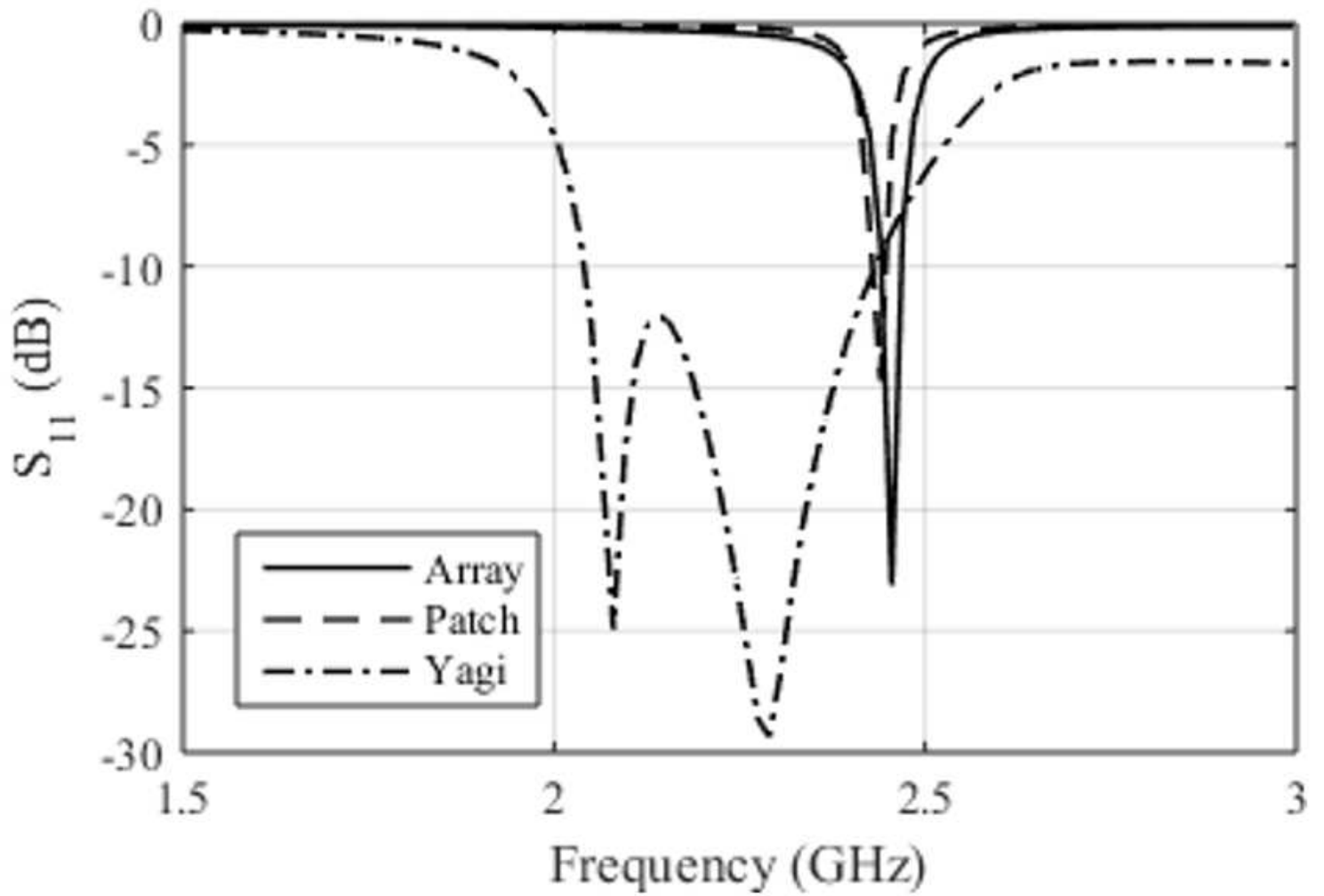
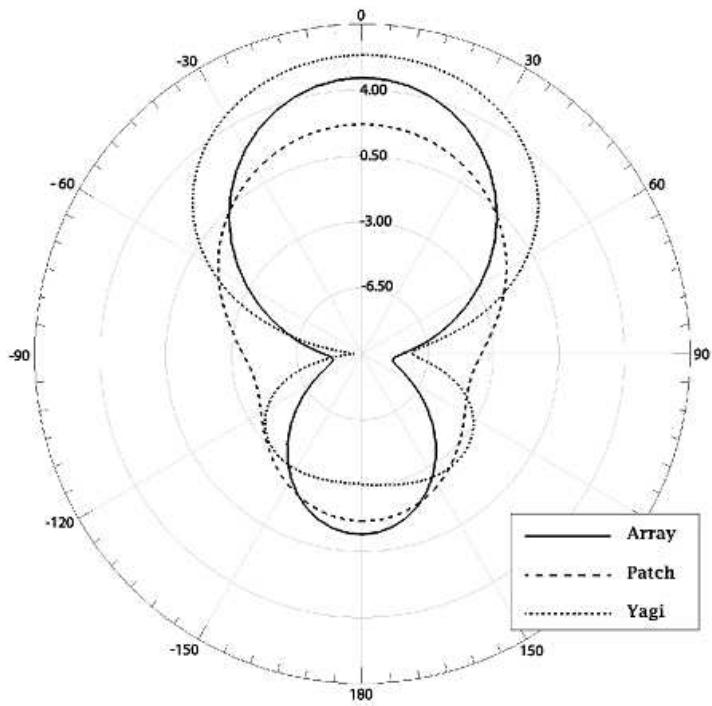
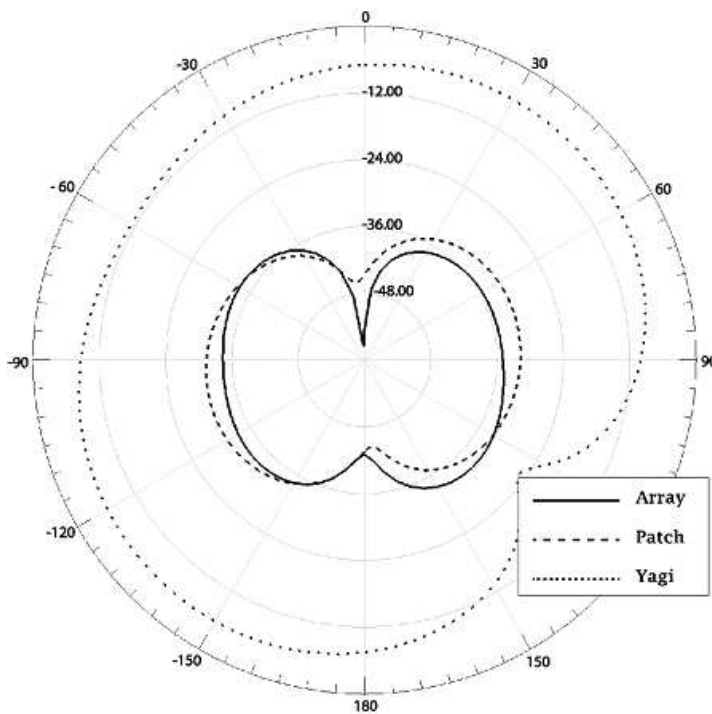


Figure 1

Reflection coefficient for the three antennas analyzed.



(a)



(b)

Figure 2

Radiation diagrams: (a) co-polarization e (b) cross-polarization.

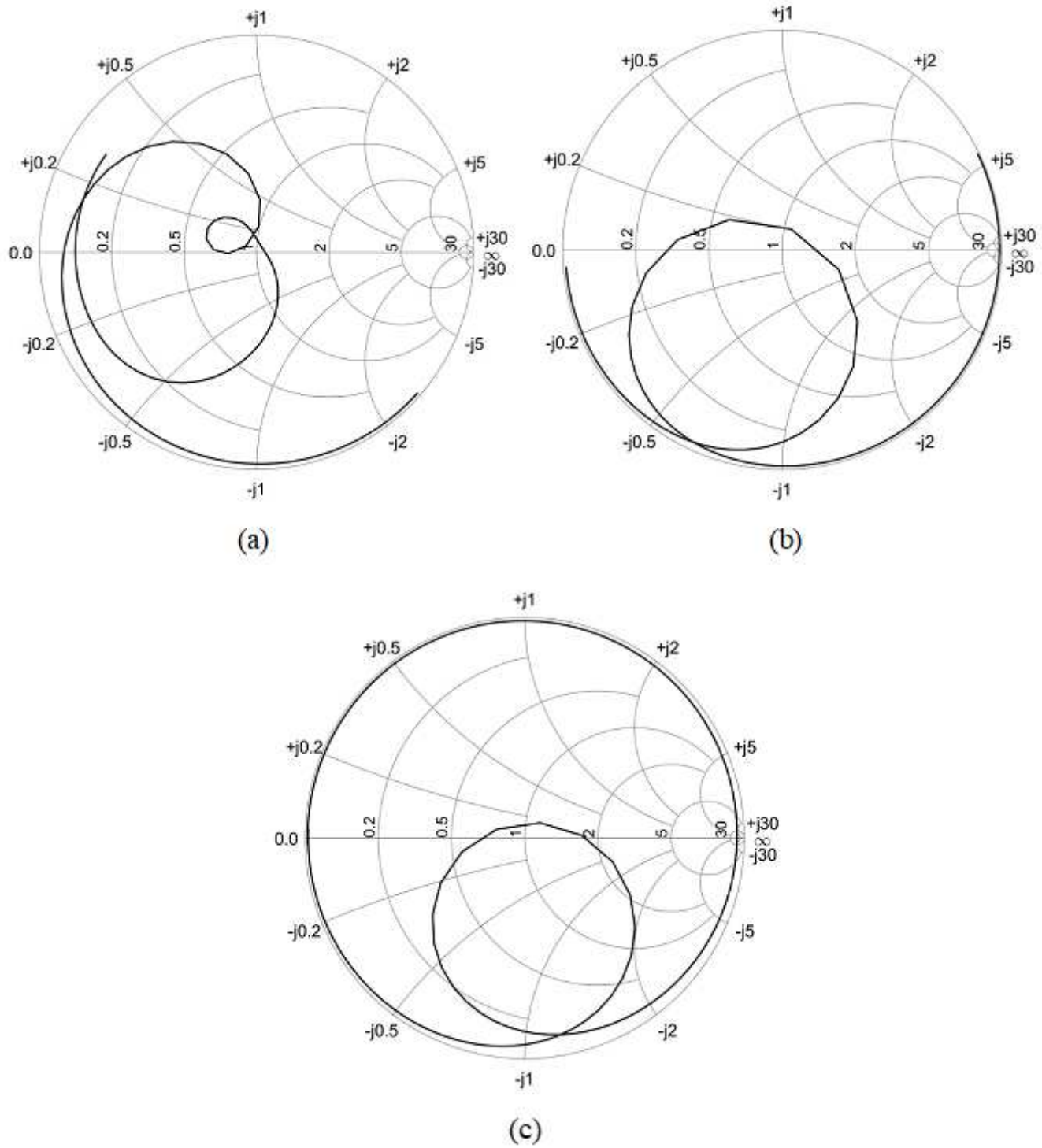


Figure 3

Smith chart: (a) Yagi antenna, (b) Patch antenna and (c) Antenna array.

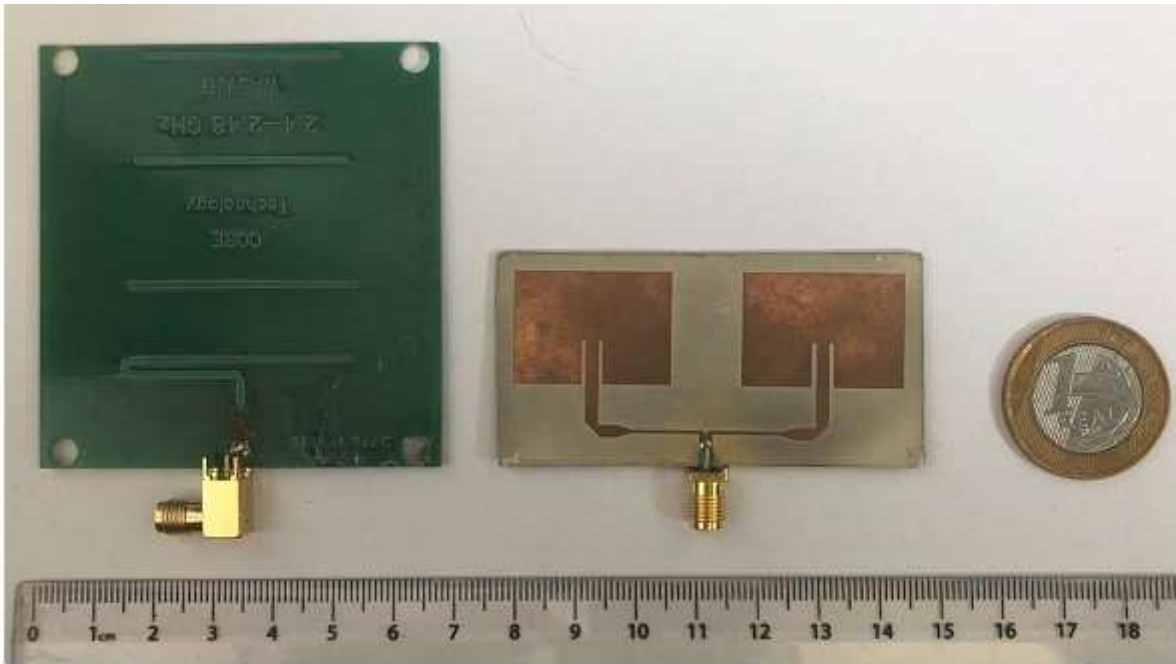


Figure 4

Yagi antenna currently in use compared in scale to the antenna array.

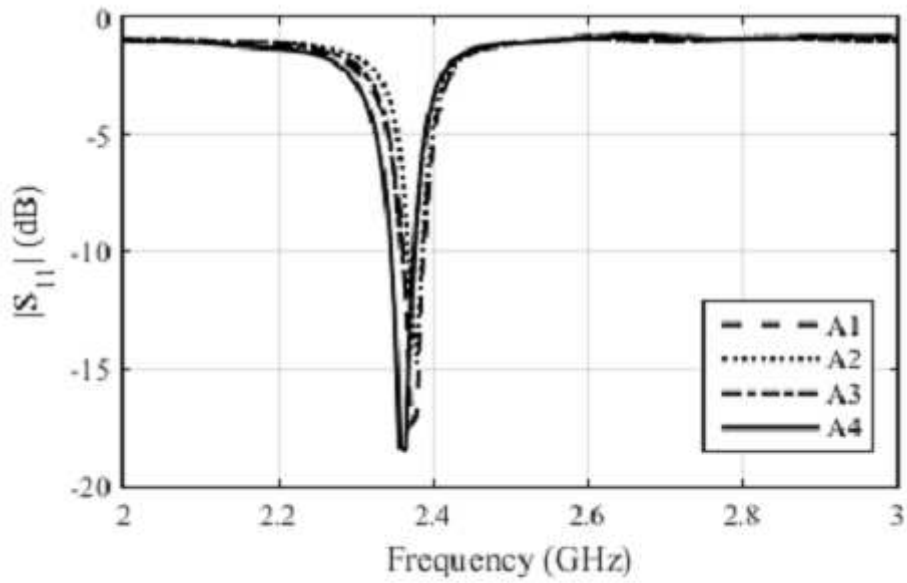


Figure 5

S11 measure for the four constructed antenna arrays.

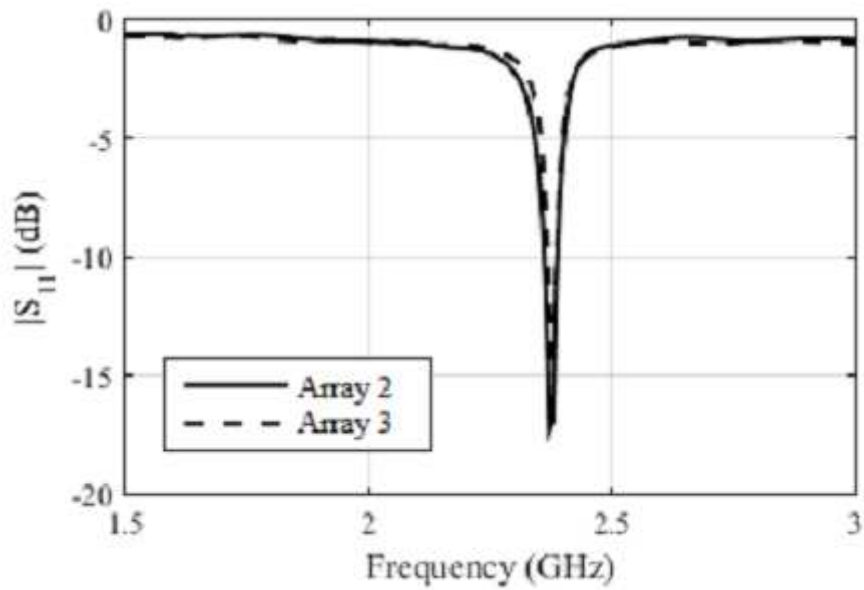


Figure 6

S11 for the antenna arrays 2 and 3 constructed.

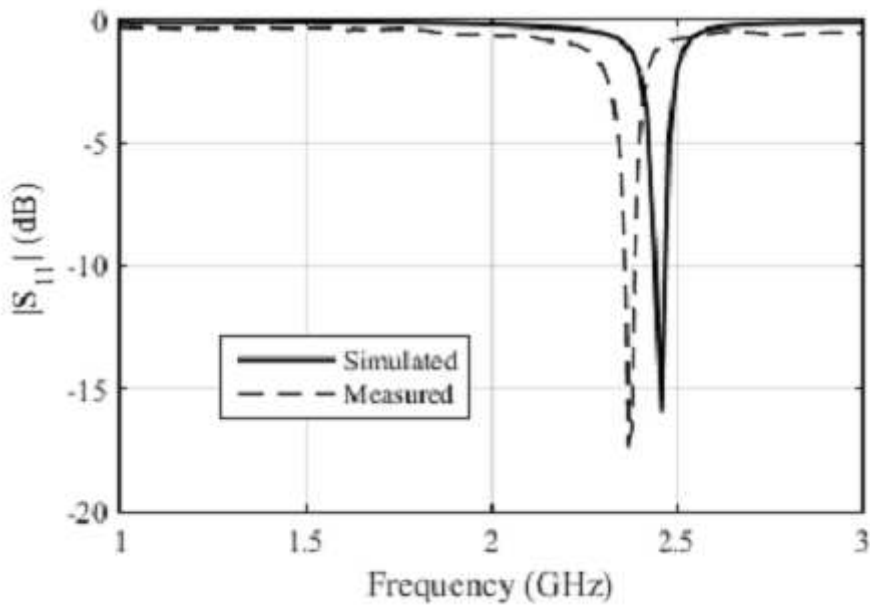


Figure 7

Comparison between the simulated and measured S11 for antenna array 2.

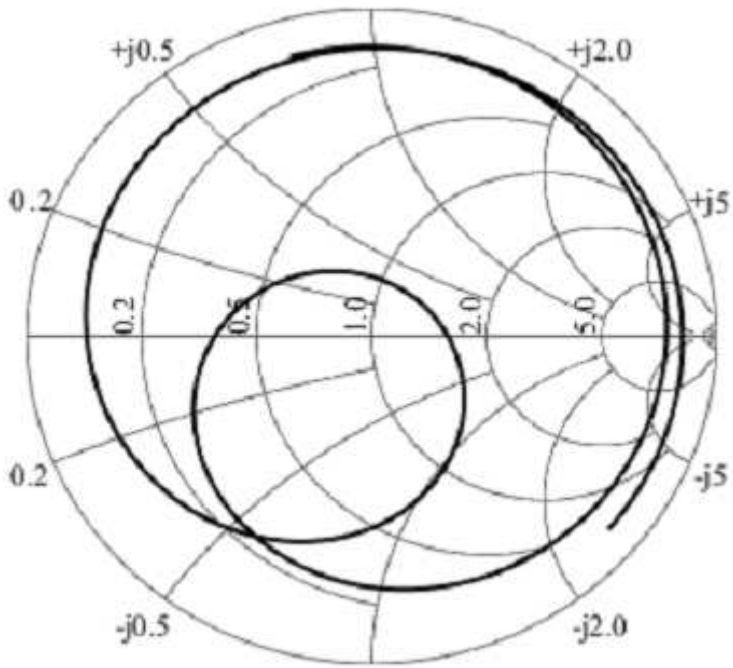


Figure 8

Smith chart for constructed antenna array 2.

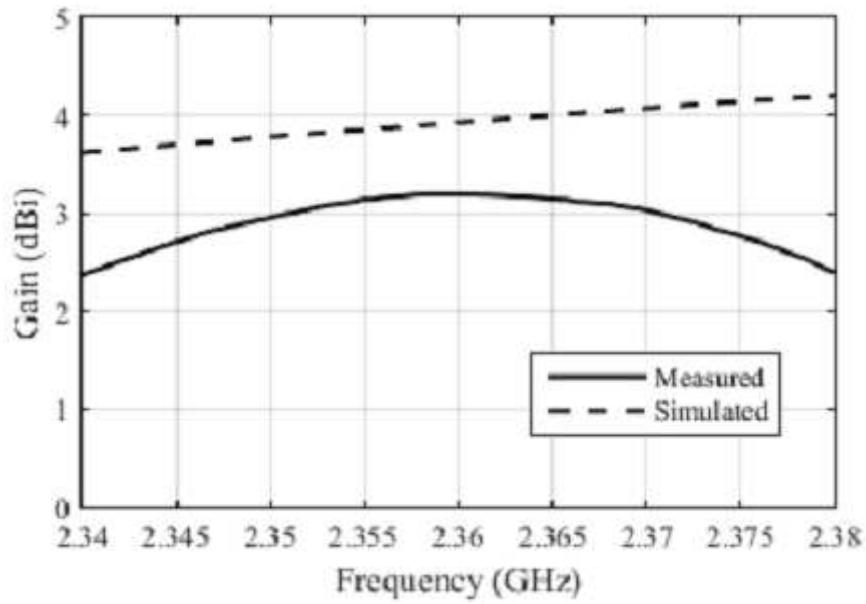


Figure 9

Comparison between the simulated and measured gains for the constructed antenna array 2.



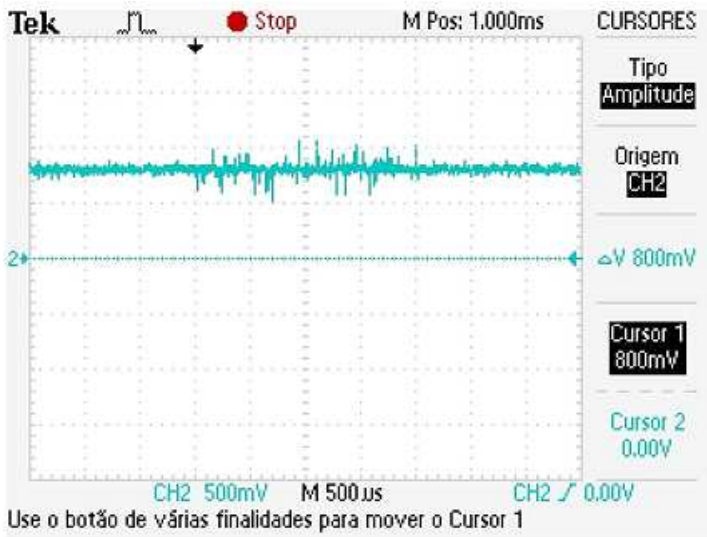
(a)



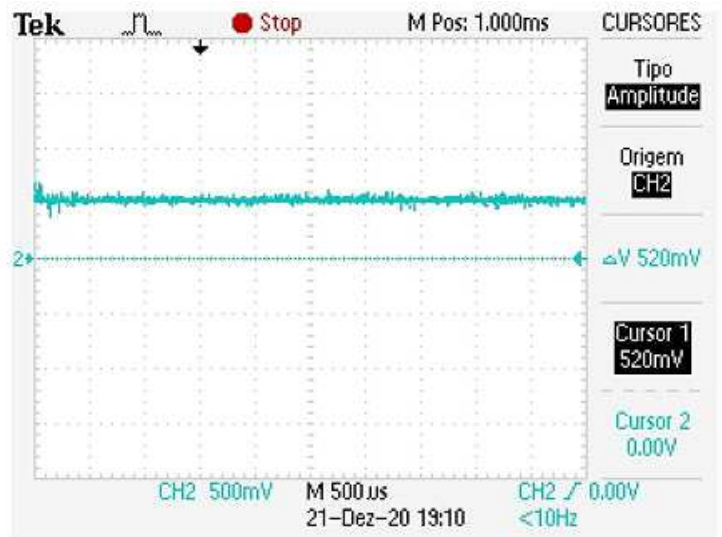
(b)

Figure 10

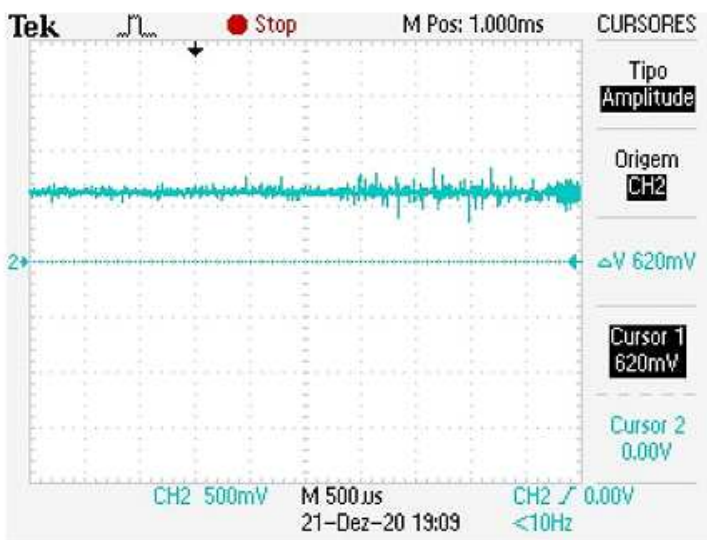
Insertion of middle finger in positions: (a) correct and (b) rotated.



(a)



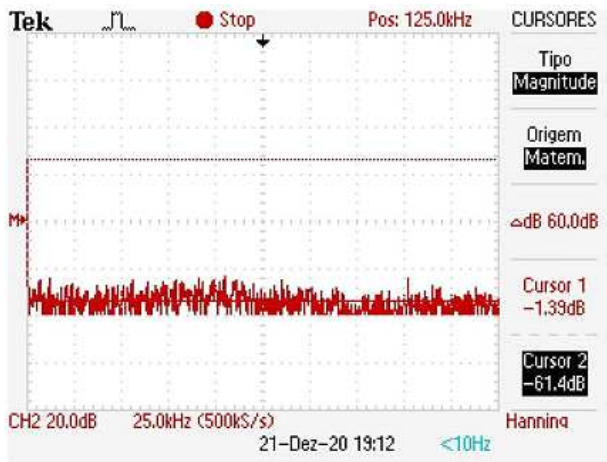
(c)



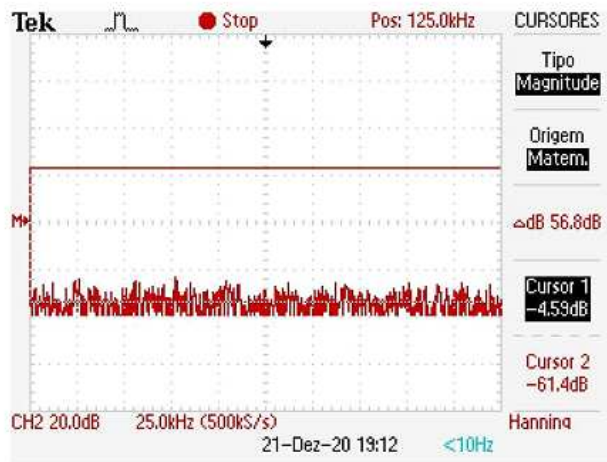
(b)

Figure 11

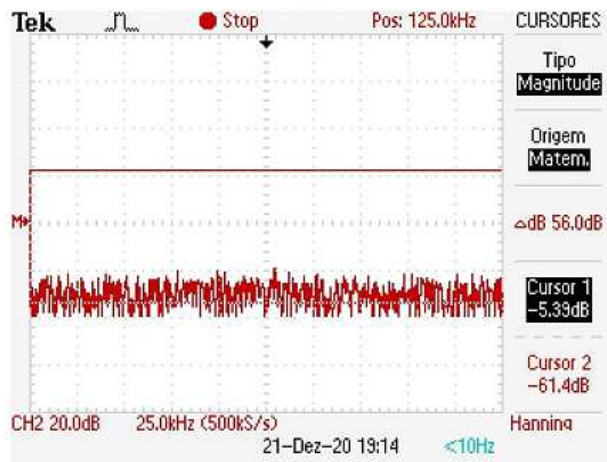
Reading of the DC level of the received signal for the first version of the Osseus: (a) without finger, (b) with finger in the correct decision e (c) with the finger in the rotated position.



(a)



(b)



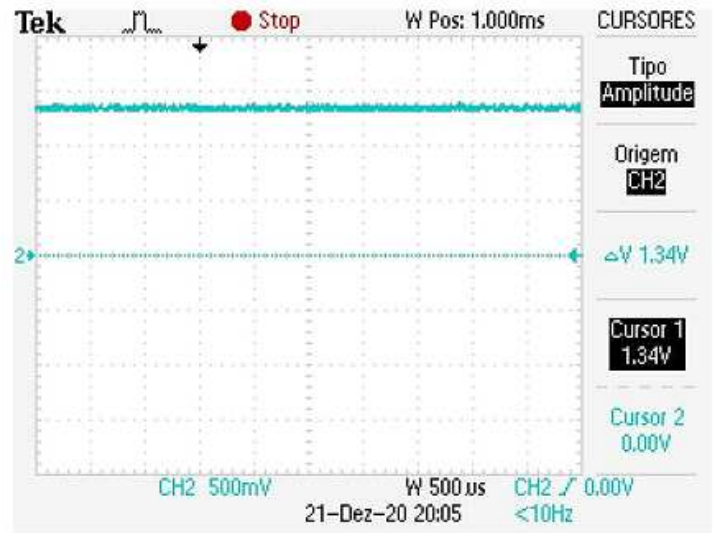
(c)

Figure 12

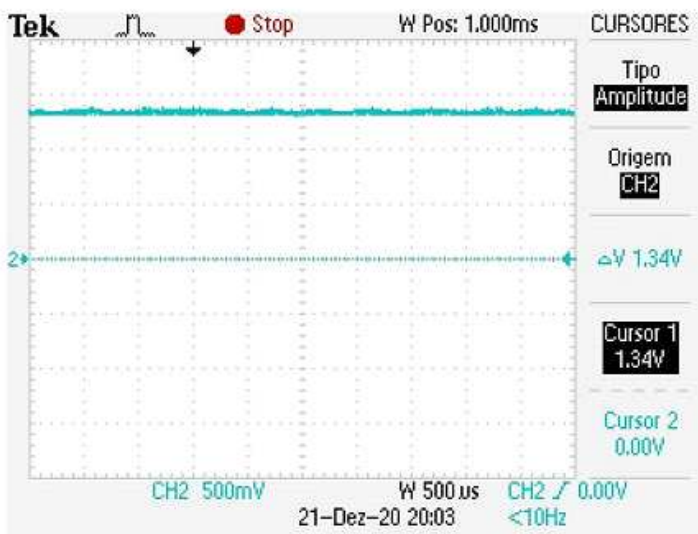
Reading of the noise level in frequency domain for the first version of the Osseus: (a) without finger, (b) with finger in the correct decision e (c) with the finger in the rotated position.



(a)



(c)



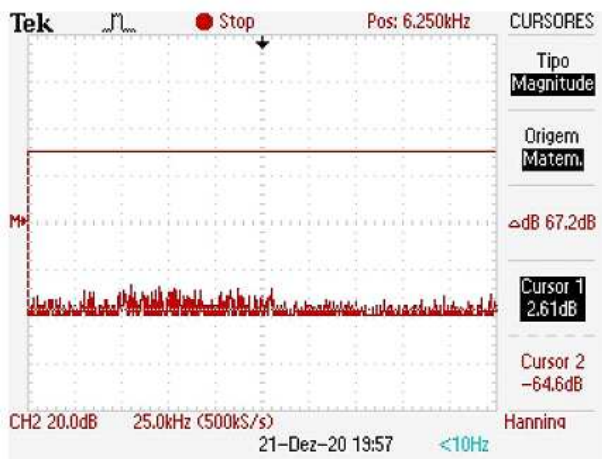
(b)

Figure 13

Reading of the DC level of the received signal for the second version of the Osseus: (a) without finger, (b) with finger in the correct decision e (c) with the finger in the rotated position.



(a)



(b)



(c)

Figure 14

Reading of the noise level in frequency domain for the second version of the Osseus: (a) without finger, (b) with finger in the correct decision e (c) with the finger in the rotated position.



Figure 15

Yagi-Uda antenna analyzed.

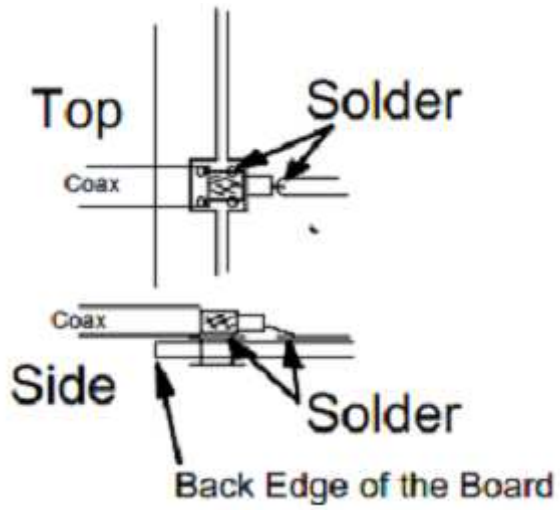


Figure 16

Connection between the coaxial cable and the Yagi-Uda antenna analyzed.

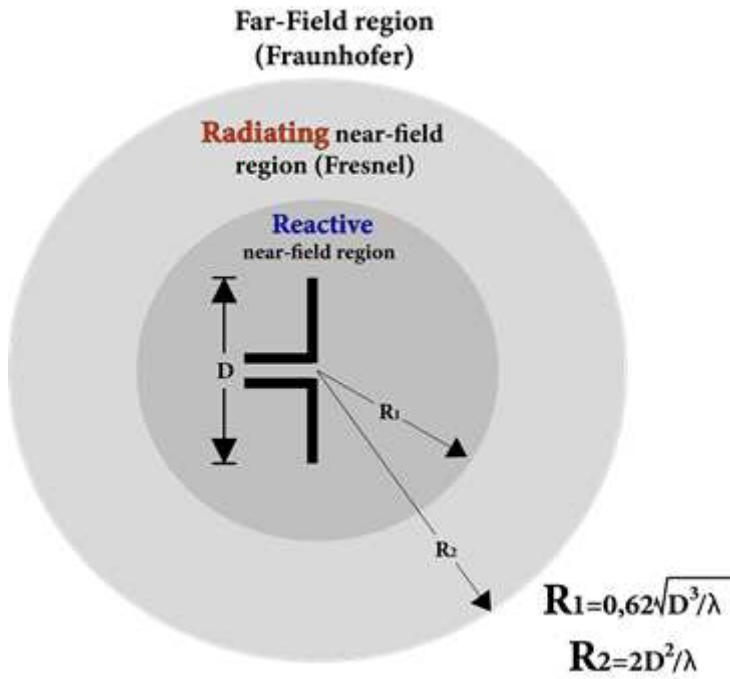


Figure 17

Near field and far field regions.

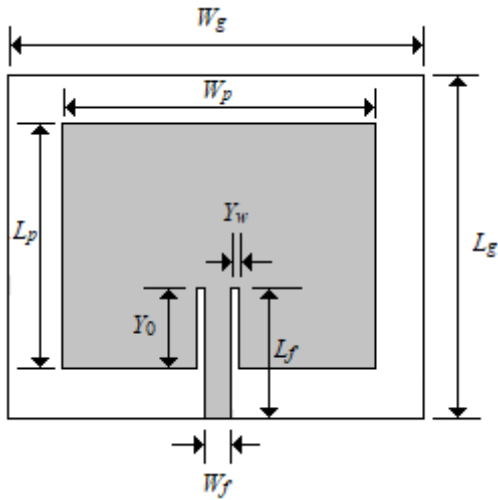


Figure 18

Antena patch de microfita.

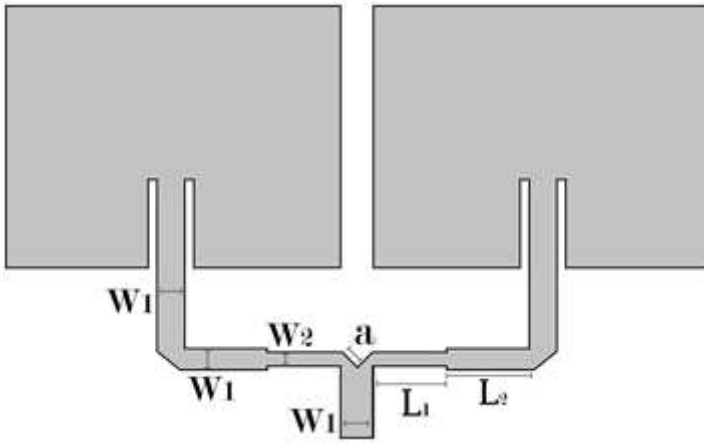


Figure 19

Antenna array and its proposed network feed.

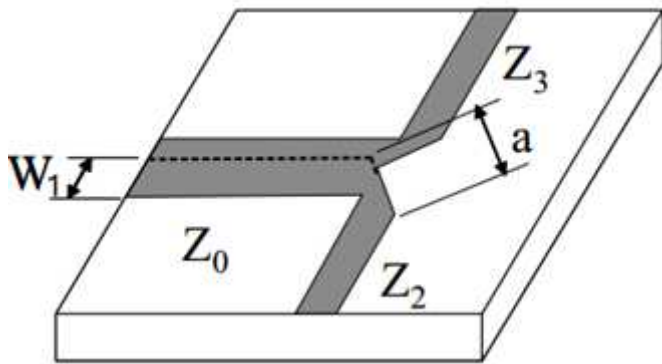


Figure 20

T-type junction.

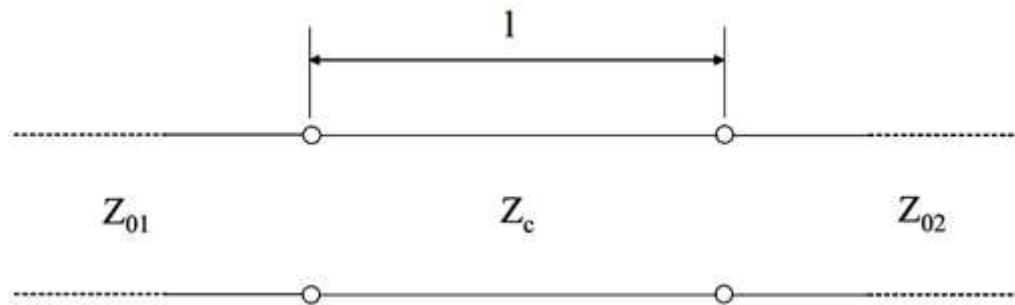


Figure 21

Insertion of $\lambda/4$ transformer.